UNIVERSITY OF OSLO
Department of
Geosciences -
Meteorology and
Oceanography section.

Determining the kinetic energy spectrum in the upper ocean

Master thesis in Geosciences Meteorology and Oceanography

Rafael Escobar Løvdahl

1st September 2011

Abstract

The turbulent dynamics of the upper ocean is a topic widely discussed by scientists. Previous investigations have shown support for two main theories; the surface quasi-geostrophic theory and the two dimensional turbulence theory. In this thesis we used statistical methods such as velocity spectra and velocity structure functions with direct oceanic measurements in the upper Atlantic ocean. At scales smaller than the deformation radius, the energy spectra and structure functions are consistent with a forward enstrophy cascade, as in two dimensional turbulence. We do not, on the other hand see any clear indications of an upscale energy cascade, despite that the peak in the energy spectrum is above the deformation radius. Whether the latter is due to an inverse cascade or direct forcing (e.g. by the Gulf Stream pinching off rings) is unclear. The results thus support two dimensional turbulence theory, rather than surface quasi-geostrophy.

Acknowlegdements

I would like to thank my supervisor Joseph Henry LaCasce and my co-supervisor Pål Erik Isachsen for their patient and encouraging guidance throughout the work with this thesis. You are great! I would also like to thank all the helpful and supporting people of MetOs section.

Also, thanks to all my fellow students, especially my good friends Ada and Henrik, for contributing intellectually through discussions and practical help, and socially by support and encouragement.

I will of course thank Hilde for being patient and encouraging. Also big thanks to Diddi and Carolyn for reading through the thesis.

Contents

Chapter 1

Introduction

The oceans and the atmosphere are turbulent. Turbulent flows appear highly disorganized and their variables are characterized by deterministic chaos. Thus these variables are highly sensitive to their initial conditions making forecasting difficult.

Forecasting capabilities have seen a tremendous improvement in the later years, to a large degree due to increased computing power. Nevertheless, in order to achieve more accurate forecasting models, a deeper understanding of the dynamics of turbulent flows is necessary. This topic has been widely discussed and researched by scientists. Two main competing theories about the nature of the upper ocean have been posed, the quasi-geostrophic theory and the two dimensional turbulence theory.

Deterministic calculation of a chaotic variable is of limited value, thus we must focus on statistics. In this thesis, we have calculated statistical measures such as velocity spectra and structure functions, using data from a turbulent region of the Atlantic ocean, in order to examine whether two dimensional turbulence theory can be supported.

Previous research in this region of the Atlantic ocean has given ambiguous results. Le Traon al examined satellite data from this region, and obtained velocity spectra which gave support to the surface quasi geostrophic turbulence theory. Wang et al. (2010), however, researched data from the M/V Oleander Project [1], in a comparable time interval as Le Traon, and obtained velocity spectra which supports two dimensional turbulence theory.

---

[1]Olenander Project, http://www.po.gso.uri.edu/rafos/research/ole/index.html

Background

A turbulence theory based on statistics for three dimensions was launched
by Kolmogorov (1941). His work was inspired by Richardson (1922), who
first presented the idea of an energy cascade from large scales to small
scales. Further, Kolmogorov's work inspired several scientist to further
investigation on the topic. Kraichnan (1967) developed a theory for turbu-
lence dynamics in two dimensions which contained two inertial ranges.
One range where the energy cascades upscale (cascade towards larger
scales) and one range where enstrophy cascades downscale (cascade to-
wards smaller scales). Charney (1971) developed the turbulence theory
further under the quasi geostrophic approximation where he showed that
the enstrophy cascade also yields.

Many scientists have put effort into verifying the turbulence theory in the
atmosphere and ocean, but the lack of a large enough dataset to perform a
statistical analysis has been a challenge. In the 1980s a concerted observa-
tional program was undertaken to measure the kinetic energy and temper-
ature spectra in the atmosphere. Commercial aircrafts were instrumented
with velocitymeters and produced a vast amount of transects. Gage and
Nastrom (1986) published a wavenumber powerspectra in the atmosphere
based on these transects, which showed clear evidence of turbulent iner-
tial ranges with $k^{-5/3}$ and k^{-3} for wavelengths ranges of 1000 km to 10
km and 1000 km to 3000 km, respectively. Gage and Nastrom sugges-
ted the k^{-3} energy spectrum to be a sign of enstrophy flux from longer
to shorter wavelengths. Lindborg (1999) applied structure functions study-
ing the same dataset as Gage and Nastrom finding a good correspondence
between structure functions and spectral analysis in the study of energycas-
cade. Lindborg further explained the k^{-3} as an direct enstrophy cascade
inherent in two dimensional turbulence theory. However, he could not ex-
plain the $k^{-5/3}$ as an upscale energy cascade.

In the ocean, Stammer (1997) estimated the kinetic energy spectra from
satellite altimetry data. His results were unable to give any information on
the smaller scales (less than 100 km), the scales which are of central interest
with regards to parameterization. Robert B. Scott (2005) used high-quality
measurements for sea surface height in the South Pacific Ocean to calculate
energy fluxes, finding a net inverse energy cascade supporting two dimen-
sional turbulence theory but no estimate on enstrophy flux for the smaller
scales were made.

Until recently, no kinetic energy spectra where calculated from direct meas-
urements of velocities from the ocean comparable to the spectra obtained
by Gage and Nastrom. But The Oleander project has instrumented a mer-
chant ship with an acoustic Doppler current profiler (ADCP) to measure
currents in the Atlantic Ocean. These measurements have provided vast
amounts of transects that make statistical analysis of the data possible. The

ADCP is set to record approximately every 2.4 km. With this resolution we can study wavelengths down to 5 km making it possible to study the smaller scales. Initial calculations on the data by Wang et al. (2010), indicate a turbulent inertial range supporting two dimensional turbulence theory.

Purpose of study

In this thesis, data provided by the Oleander project has been analyzed. This is the same data set used by Wang et al. (2010) to calculate the velocity spectra for the total region of measurements. In this thesis, however, in addition to calculating the entire regions of measurements, we have also calculated the velocity spectra of two sub-regions, one in the western region where the Gulf Stream is located, and one in the eastern region outside of the Gulf Stream. The calculations have been done from 55 m, 155 m and 305 m records.

The purpose of dividing the region in the horizontal and vertical, is to make it possible to examine the influence of the Gulf Stream, as well as to supply information on the validity of the assumptions of isotropy and homogeneity, which are central in two dimensional turbulence theory.

Both spectral analysis and structure functions have been used in the investigation. The structure functions, which are moments of velocity differences between separated points in space, have been used in prior turbulence studies (Lindborg, 1999) (Frisch, 1995), but have not been used on data from the Oleander Project earlier.

The results from the structure functions have been compared to the theoretical predictions of two dimensional turbulence theory. The advantage of using structure functions rather than a spectral analysis, is that they provide a much more direct connection between scale and the actual measurement. Also, there is no need of removing mean values nor to detrend the data. On the other hand, spectral analysis can give better information on the energy and enstrophy contents within a certain wavenumber interval.

By using both structure functions and spectral analysis, we intend to present a complementary view on the turbulence in the upper ocean. The data from the Oleander Project are one dimensional, and are not suited for direct flux calculations. However, the third order structure functions contain information on the fluxes and have been used to make inferences about the fluxes.

All methods have been tested on a two dimensional model data set prior to the calculations on the oceanic data. This has been done in order to validate

and examine the response of the methods in a known dynamical system.

This thesis is divided into six chapters. Following the introduction, relevant theory is presented in chapter 2. Then, a description of the data set as well as the methods, are described in chapter 3. This chapter also includes the results from the test of the methods. In chapter 4, the results obtained from applying the methods on the Oleander data are presented. Chapter 5 provides a discussion of the results. Finally, chapter 6 concludes and summarizes.

Chapter 2

Theory

This chapter starts with a general presentation of turbulence followed by a short description of the statistical approach to turbulence and goes through the important dynamics and implications related with two dimensional turbulence.

2.1 Turbulent flows

Figure 2.1: The volcano Grímsvötn in Island erupting spring 2011 showing massive turbulent advection. Picture by Ólafur Sigurjónsson.

Figure 2.1 shows a smoke plume from an erupting volcano as an example of a turbulent flow. From the picture it is seen that the motion is chaotic and random, making it impossible to predict the motion of the particles driven by the flow. Turbulent flows are not necessarily as violent as a volcano eruption. They can be found in all sorts of fluids under the right conditions, like stirred tea cups.

The energy received from the sun is not evenly distributed, and has more input at equatorial regions. This unbalanced energy input drives the earth's dynamical system, reflecting nature's strive to even out energy differences. This is mediated by turbulent flows which effectively transport and distribute energy.

Turbulence has been observed and studied by scientists for a long time, but still its complexity leaves this feature of nature without a clear definition. However, there are three clear, well known characteristics inherent in turbulent flows.

- the flow is random and chaotic in space and time

- big Reynolds number $Re = \frac{Ud}{\nu} > O(10^3)$
  (U is the dominant velocity in the eddy, d is the size of the eddy and ν is the viscosity)

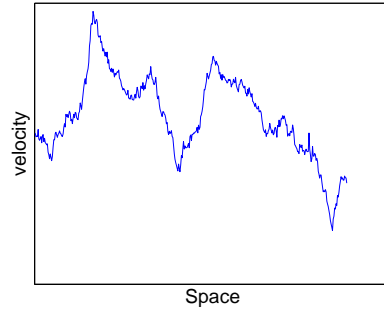- interaction between different length scales

Figure 2.2: Unpredictable motion.

An example of a random variable is presented in figure 2.2. Using statistics based on the random variable it is possible to predict what may seem as a completely unpredictable motion. Following Reynolds decomposition, the variable can be divided into a mean and a fluctuating part

$$u = \bar{u} + \acute{u} \tag{2.1}$$

Assumed the variable u is a time dependent variable, the fluctuations will go to zero when averaging over a time interval much greater than the space time of the fluctuation itself

$$\bar{\acute{u}} = 0 \tag{2.2}$$

This way the equations of motion may still be used in order to predict the future behavior of a random variable. The equation that governs the turbulent flow of an incompressible fluid is the Navier Stokes equation:

$$\frac{\partial}{\partial t}\vec{v} + \vec{v}\nabla \cdot \vec{v} = -\frac{1}{\rho_0}\nabla p + \nu\nabla^2\vec{v} \tag{2.3}$$

$$\nabla \cdot \vec{v} = 0 \tag{2.4}$$

Taking a closer look at (2.3), the second term on the r.h.s. is nonlinear. When dividing the variable of (2.3) as in equation (2.1), this nonlinearity presents challenges for the predictability of turbulent fluid motion and is referred to

as 'the closure problem' which makes the unknowns outnumber the equations. It also gives rise to the interaction between different length scales referred to as triad interactions.

Applying statistical theory and performing ensemble averages is a challenging task on real data. Nature is not likely to repeat itself and exhibit the same conditions for each event in order to get a representative average for the events. The theories presented for turbulence based on statistics meet this challenge by making assumptions.

2.2 Assumptions and statistics in turbulence

Assumptions

The turbulence theories that will be presented in this thesis are based on a statistical approach to turbulence. This approach is valid under certain assumptions presented here. This makes it possible to get a solution for the random velocity $+vecv$ using the Navier Stokes equation under turbulent conditions.

- **Stationarity**
  Turbulence is stationary if the mean of the variables are time independent, and the variables are **ergodic** if the time averages converge to the mean as the time goes to infinity

$$\frac{1}{T} \int_0^T v(t), dt = <v> \, as \, T \to \infty \tag{2.5}$$

  In this case a time average is equivalent to an ensemble average.

- **Homogeneity**
  Turbulence is homogeneous if the mean of the variables are space independent, meaning that turbulence fills all space. Then from ergodicity the ensemble average can be calculated as a spatial average

$$\frac{1}{L} \int_0^L v(x), dx = <v> \, as \, L \to \infty \tag{2.6}$$

- **Isotropy**
  Turbulence is isotropic if it is independent of direction. A modified version of this assumption is *local isotropy*, which assumes isotropy in a limited range of scales. This implies that the anisotropy at larger scales is not transferred to smaller scales by triad interactions (2.3), leaving smaller scales isotropic.

- **Self-similarity**
  In a self-similar system, the properties of the variables enclosed by

the equations of turbulent motion are independent of scale. Figure 2.3 (a) shows the self-similar Brownian motion curve containing the phenomena of scale invariance. By zooming in on the function of two different scales, its shape remains unaffected.

          (a)   **(b)**
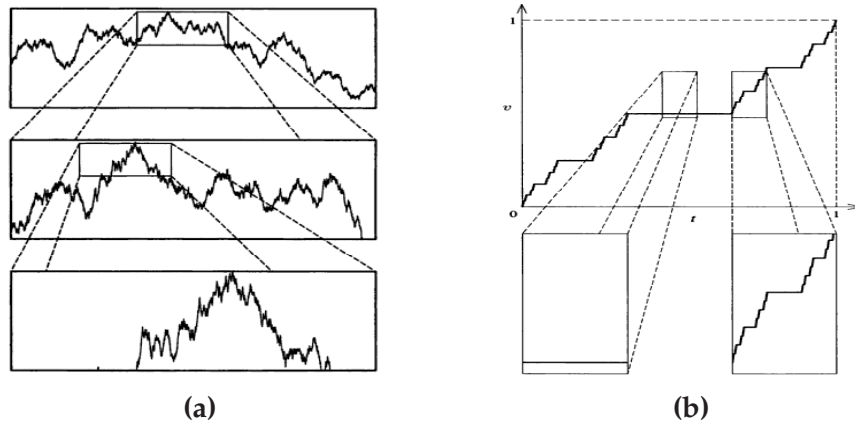
Figure 2.3: *Brownian motion curve (a) enlarged twice, illustrating its self-similarity by keeping its characteristic motion intact completely independent of scale. In (b), the Devil's staircase. This is a function showing intermittency because when enlarged the shape of the function is not conserved. Picture from Frisch (1995)*
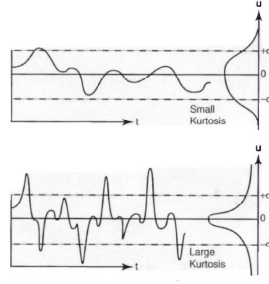
Intermittency

Spatial intermittency is present in a function when it displays localized regions of large magnitude separated by wide regions of smaller magnitude. Presented in figure 2.3 (b) is a function of intermittent character. The function exhibits a completely different behavior at different scales as shown under magnification of a parcel of the function. This means that the shape of the function at one scale is not representative for the shape of the function at different scales.

The **kurtosis** is a measure for intermittency, defined as the fourth order moment of the function, normalized by the variance:

$$kurtosis = \frac{< f^4 >}{< f^2 >^2} \tag{2.7}$$

If the kurtosis is small and constant on the resolution of the function, it is a sign of the function being self similar (Frisch, 1995). The value of the kurtosis is an estimate of how the measurements are spread around the mean value. Large value is a sign of extreme events, and can cause the higher order statisitcs to converge slower than the lower order statistics. Figure (2.4) [1] presents two functions of different kurtosis. Functions with a Gaussian probability distribution have a kurtosis equal to 3.

---

[1]http://ocw.mit.edu/courses/earth-atmospheric-and-planetary-sciences/12-820-turbulence-in-the-ocean-and-atmosphere-spring-2007/lecture-notes/

Figure 2.4: Two functions and theri PDFs. Upper picture shows a function with small kurtosis. Lower picture shows a figure with large kurtosis. Figure obtained from MITOPENCOURSEWHARE.

Statistics

Statistical tools became very important when it was discovered that the random and chaotic variables showed predictable statistics. The statistical approach to turbulence has produced the theories which will be presented later in this chapter.
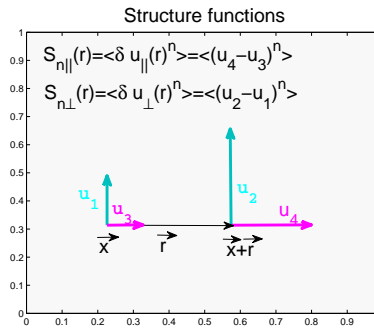
Structure functions

In order to present structure functions it is reasonable to start by defining a velocity increment (Frisch, 1995):

$$\delta u(\vec{x}, \vec{r}) \equiv [\vec{u}(\vec{x} + \vec{r}) - \vec{u}(\vec{x})] \cdot \frac{\vec{r}}{r} \tag{2.8}$$

where $\vec{r}$ is the separation between the velocity $\vec{u}$ at points $\vec{x} + \vec{r}$ and $\vec{x}$. The term $r = |\vec{r}|$ projects the velocity increment onto the line of separation. A longitudinal velocity increment measures velocities aligned with $\vec{r}$, and the transverse velocity increment measures velocity perpendicular to $\vec{r}$.

Structure functions are velocity increments to the nth power, averaged over the ensemble of velocities. The turbulence theory discussed in this thesis, assumes the turbulence to be isotropic and homogeneous. Thus, under this premise, the vectors in (2.8) can be replaced by scalars and $\vec{x}$ is left out. The structure function of nth order takes the form:

$$S_n(r) \equiv < (\delta u(r))^n > \tag{2.9}$$

Figure 2.5: $u_{||}$(pink) and $u_\perp$(green) at $\vec{x}$ and $\vec{x} + \vec{r}$

which only depends on the separation between the observations. Longit-
udinal and transverse structure functions are defined as:

$$S_{n||}(r) = < \delta u_{||}(r)^n > = < (u_{||}(\vec{x}+r) - u_{||}(\vec{x}))^n > \qquad (2.10)$$

$$S_{n\perp}(r) = < \delta u_{\perp}(r)^n > = < (u_{\perp}(\vec{x}+r) - u_{\perp}(\vec{x}))^n > \qquad (2.11)$$

Energy spectra

Analyzing stationary random functions, energy spectra indicate the energy
distribution of the functions in wavenumber space. It is based on Fourier
theory which allows a stationary function ($v(\vec{r})$) to be written as a sum of
waves:

$$v(\vec{r}) = \sum_{\vec{k}} \hat{v}_{\vec{k}} e^{i\vec{k}\cdot\vec{r}} \qquad (2.12)$$

where $\vec{k}$ is the wavenumber related to the the waves. With this description
of $v(\vec{r})$, it is possible to divide the function in two parts, one part consist-
ing of the waves with k $\leq$ K and one part consisting of the waves with k >
K. Both are illustrated in figure 2.6. The former is defined as a low-passed
signal and the latter as a high-passed signal.

(a)

(b)

(c)
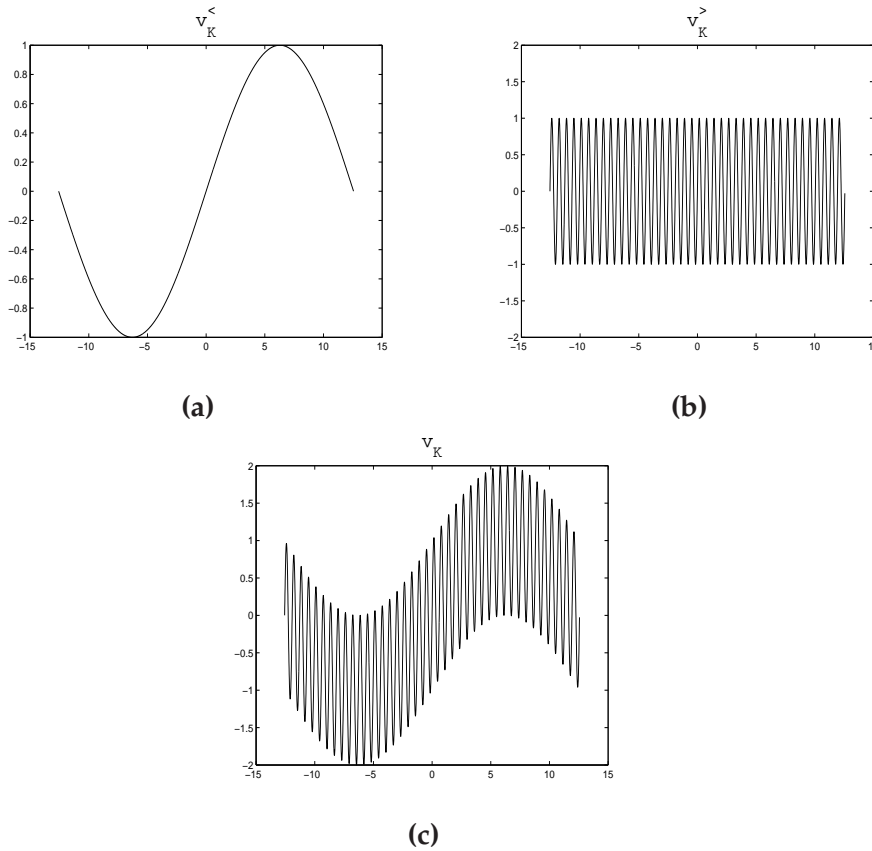
Figure 2.6: *Lowpassed (a) highpassed (b) and total signal (c).*

Following Frisch (Frisch, 1995), the spatial cumulative energy spectrum is defined:

$$\mathcal{E}(K) \equiv \frac{1}{2} < |\vec{v}_K^{<}(\vec{r})|^2 >, \tag{2.13}$$

where $\vec{v}_K^{<}$ is the low-passed filtered component of $\vec{v}_K$, containing all waves with wavenumbers less or equal to K. Further, the spectral density at k is defined as:

$$E(k) \equiv \frac{d}{dk}\mathcal{E}(k) \geq 0 \tag{2.14}$$

From empirical results, the energy spectra of turbulent flows often follow a power-law. Therefore, assuming that an energy spectrum follows a power-law:

$$E(k) = C|k|^{-n}, C > 0 \tag{2.15}$$

the stationary random functions only have a finite variance for certain values in the range, $n \in [1,3)$. Also, there can be established a relation between the second order spatial structure functions when the velocity increments are homogeneous and goes like (Frisch, 1995):

$$< |(\delta u(r))^2| > \propto |r|^{n-1} \tag{2.16}$$

2.3   Triad interactions

The energy a turbulent flow receives from forcing at a certain scale, will not pile up at this scale. This energy cascades to other scales, which rearranges the energy spectral distribution. Boffetta (2007) showed this by numerical simulations of energy cascades. These numerical simulations can be related to the motion in the upper ocean. The eddies are primarily forced by energy from the baroclinic instability, which scale as the deformation radius.

The energy cascade arises from interaction of different wavelengths. This is shown next, by studying energy in spectral space. An energy equation is found by adding forcing to equation (2.3):

$$\frac{\partial}{\partial t}\vec{v} + \vec{v} \cdot \nabla\vec{v} = -\nabla(\frac{p}{\rho_0}) + F + \nu\nabla^2\vec{v} \tag{2.17}$$

Further manipulation of the momentum equation will show that the forcing term is responsible for injecting energy into the system while the dissipation terms removes it.

The fluid studied was assumed incompressible (2.4), so the advection term can be rewritten:

$$\frac{\partial}{\partial t}\vec{v} + \nabla \cdot (\vec{v}\vec{v}) = -\nabla(\frac{p}{\rho_0}) + F + \nu\nabla^2\vec{v} \tag{2.18}$$

This equation dotted with the velocity becomes:

$$\frac{\partial}{\partial t}\frac{|\vec{v}^2|}{2} + \nabla \cdot \frac{(\vec{v}|\vec{v}^2|)}{2} = -\nabla \cdot \vec{v}(\frac{p}{\rho_0}) + F \cdot \vec{v} + \nu\vec{v} \cdot \nabla^2\vec{v} \qquad (2.19)$$

Kinetic energy is defined as $E = \frac{|\vec{v}^2|}{2}$, a quantity recognized in the previous equation, which enables the term on l.h.s of (2.19) to be written as:

$$\frac{D}{dt}E = -\nabla \cdot \vec{v}(\frac{p}{\rho_0}) + F \cdot \vec{v} + \nu\vec{v} \cdot \nabla^2\vec{v} \qquad (2.20)$$

where $\frac{D}{dt} = \frac{\partial}{\partial t} + \vec{v} \cdot \nabla$. To capture the impact of forcing and dissipation in the energy budget, we integrate (2.19) over an idealized volume specified as:.

- A domain enclosed by solid walls

- a periodic domain

- an infinite domain

Performing this integration, the first term on the r.h.s of (2.19) will vanish from Gauss's theorem due to the boundary conditions of a periodic domain. The result of the integration is:

$$\frac{D}{Dt}E = \int\int\int \vec{v} \cdot F\, dV + \nu\int\int\int \vec{v} \cdot \nabla^2\vec{v}\, dV \qquad (2.21)$$

where $E = \int\int\int \frac{|\vec{v}^2|}{2}dV$ is the total energy of the fluid.

One of the features in the dissipation term (second term on the r.h.s) can be transformed into:

$$\nabla^2\vec{v} = \nabla(\nabla \cdot \vec{v}) - \nabla \times (\nabla \times \vec{v}) = -\nabla \times \vec{\omega} \qquad (2.22)$$

so:

$$\nu\int\int\int \vec{v} \cdot \nabla^2\vec{v}\, dV = -\nu\int\int\int \vec{v} \cdot (\nabla \times \vec{\omega})\, dV \qquad (2.23)$$

then by a vector identity yields:

$$\nu\int\int\int [\vec{\omega} \cdot (\nabla \times \vec{v}) + \nabla \cdot (\vec{\omega} \times \vec{v})]\, dV \qquad (2.24)$$

where the divergence term is zero and the time change in the total energy follows:

$$\frac{D}{dt}E = -\nu\int\int\int |\vec{\omega}|^2\, dV + \int\int\int \vec{v} \cdot F\, dV \qquad (2.25)$$

These results allow us to determine the role of dissipation and forcing in the change of total energy. The quantity $|w|$ is always positive so the dissipation term will always be negative. This means that dissipation removes energy from the system and makes the total energy decrease. The forcing

term will inject or remove energy from the system depending on the direction of the forcing relative to the velocity.

To ensure capturing the transport mechanism, we study a range of scales far lesser than where forcing occurs and far greater than where dissipation occurs. In this range known as intermediate scale, the momentum equation without rotation nor gravitation becomes:

$$\frac{\partial}{\partial t}\vec{v} + \vec{v}\cdot\nabla\vec{v} = -\nabla(\frac{p}{\rho_0}) \tag{2.26}$$

Taking the divergence will leave the time derivative out and the equation becomes:

$$\nabla\cdot(\vec{v}\cdot\nabla\vec{v}) = -\nabla^2(\frac{p}{\rho_0}) \tag{2.27}$$

which can be written

$$\frac{\partial^2 p}{\partial x_i^2} = -\rho_0\frac{\partial u_i}{\partial x_j}\frac{\partial u_j}{\partial x_i} \tag{2.28}$$

solving this for p and expressing it in the spectral space by Fourier transformation using the convolution theorem:

$$\frac{1}{V}\int\int\int u_i(\vec{x},t)u_j(\vec{x},t)e^{i\vec{k}\cdot\vec{x}}d\vec{x} = \frac{1}{(2\pi)^3}\int\int\int \hat{u}_i(\vec{q},t)\hat{u}_j(\vec{p},t)\delta(\vec{p}+\vec{q}-\vec{k})d\vec{p}d\vec{q} \tag{2.29}$$

$$p \Longleftrightarrow \rho_0\int\int\int\frac{q_j p_i}{k^2}\hat{u}_j(\vec{p},t)\hat{u}_i(\vec{q},t)\delta(\vec{p}+\vec{q}-\vec{k})d\vec{p}d\vec{q}, \tag{2.30}$$

and the advection term in spectral space:

$$u_j\frac{\partial u_i}{\partial x_j} \Longleftrightarrow i\int\int\int q_j\hat{u}_j(\vec{p},t)\hat{u}_i(\vec{q},t)\delta(\vec{p}+\vec{q}-\vec{k})d\vec{p}d\vec{q}, \tag{2.31}$$

The momentum equation (2.26) in spectral space is:

$$\frac{\partial}{\partial t}\hat{u}_i(\vec{k},t) = -i\int\int\int q_j(1-\frac{p_i k_i}{k^2})\hat{u}_j(\vec{p},t)\hat{u}_i(\vec{q},t)\delta(\vec{p}+\vec{q}-\vec{k})d\vec{p}d\vec{q} \tag{2.32}$$

multiplied by $\hat{u}_i^*(\vec{k},t)$ and divide by two yields:

$$\frac{\partial}{\partial t}E(\vec{k},t) = -i\int\int\int q_j(1-\frac{p_i k_i}{k^2})\hat{u}_j(\vec{p},t)\hat{u}_i(\vec{q},t)\hat{u}_i^*(\vec{k},t)\delta(\vec{p}+\vec{q}-\vec{k})d\vec{p}d\vec{q} \tag{2.33}$$

where $E(\vec{k},t) = \frac{\partial}{\partial t}\frac{|\hat{u}_i(\vec{k},t)|^2}{2}$ is the energy at wavenumber k.

Equation (2.33) governs the energy exchange between length scales driven by triad interaction. It shows that change in energy at one scale (k) is incited by two other wavelengths (p an q). The delta function restricts the interaction only to involve three different wavelengths (k,p,l) where the sum of the two affecting wavelengths are the third affected wavelength (k=q+p).

2.4   Kolmogorov's theory of three dimensional turbulence

Kolmogorov did pioneering work in his study of turbulence. Using a statistical approach and assuming homogeneity, isotropy and only local interactions in the inertial range (scales far away from where dissipation and forcing occur), Kolmogorov derived his four-fifths law, a cornerstone in turbulence theory (Frisch, 1995).

$$< (\delta v_{||}(r))^3 >= -\frac{4}{5}\epsilon r \tag{2.34}$$

This law has been verified by several measurement in marine boundary layers (Van Atta, 1970). From Frisch (1995) the relation between structure functions of the order p from self-similarity of the Navier Stokes equation is found to be:

$$S_p(r) \propto r^{p/3} \tag{2.35}$$

Kolmogorov assumed low order statistics (structure functions up to third order) in the inertial range, only depend on ϵ and r. Thus,

$$S_p(r) = C_p \epsilon^{p/3} r^{p/3} \tag{2.36}$$

by dimensioning

$$(\epsilon r)^{p/3} = (m^3/s^3)^{p/3} \tag{2.37}$$

This gives the following relations for the second and third order structure functions in three dimensional turbulence:

$$S_2(r) \propto r^{2/3} \tag{2.38}$$

$$S_3(r) \propto r \tag{2.39}$$

The energy spectrum in the inertial range according to Kolmogorov's theory is found by dimensional analysis. Energy has units m^2/s^2 which gives the spectrum dimensions L^3/T^2. The flux of energy has units m^2/s^3 which gives the dimensions L^2/T^3. Comparing these two dimensions in the inertial range where only ϵ and lengthscale k determine the energy spectrum, Kolmogorovs five-thirds law yields:

$$E(k) \propto \epsilon^{2/3} k^{-5/3} \tag{2.40}$$

2.5 Two dimensional turbulence

In meteorology and oceanography, when describing large scale motions, the equations of motion are often simplified in two dimensions rather than using them in three dimensions. This is justified from observations in large scale motion, which show that horizontal velocities are much greater than vertical velocities. Another approach is the quasi geostrophical approximation, where the vertical velocities are assumed to be much smaller but not zero, giving a nearly two dimensional view. Quasi geostrophic turbulence and two dimensional turbulence have been shown by Charney (Charney, 1971) to be compatible. Numerical simulations (Vallgren and Lindborg, 2010) have confirmed Charney's theory on QG turbulence being much like two dimensional turbulence featuring a forward enstrophy cascade and inverse energy cascade. Three dimensional effects need to be accounted for at small scales where vertical and horizontal velocities are comparable, otherwise a two dimensional approach is functional.

2.5.1 Cascades

Consider a flow where the energy initially is concentrated at a narrow band of wavenumbers. Then, as time evolves, the energy in the narrow band of wavenumbers will be transported to other wavelengths by triad interactions. Thereby, the energy spectrum broadens as shown in figure 2.7. To show the details on how the broadening takes place in two dimensions by energy cascades, we start by arguing that there is energy conservation in two dimensions.
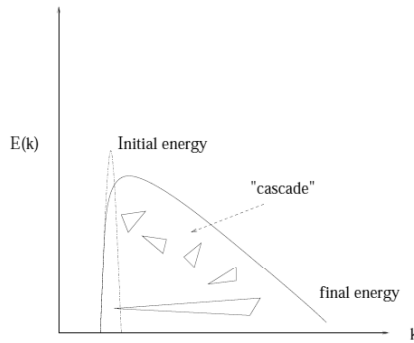
Figure 2.7: *Energy spectra of a flow before and after triad interactions have rearranged energy over the scales. Figure by J.H. Lacasce*

The equation for the total vorticity ω_a is (Holton, 2004):

$$\frac{D}{Dt}\vec{\omega}_a = \vec{\omega}_a \cdot \nabla \vec{u} + \nu \nabla^2 \vec{\omega} \qquad (2.41)$$

where ω_a is the planetary plus relative vorticity. A two dimensional velocity ($\vec{v} = (u, v, 0)$) results in a relative vorticity ($\nabla \times \vec{v}$) that has no horizontal component ($\vec{\omega} = \zeta \vec{k}$). Also the planetary vorticity is predominantly vertical. Thus, the first term on the r.h.s of (2.41) becomes zero in two dimensions:

$$\vec{\omega}_a \cdot \nabla \vec{u} = (\zeta + f)\vec{k} \cdot \nabla (u\vec{i} + v\vec{j}) = 0 \tag{2.42}$$

It then follows

$$\frac{D}{Dt}\vec{\omega}_a = \nu \nabla^2 \vec{\omega} \tag{2.43}$$

Assuming f is constant (2.43) becomes:

$$\frac{D}{Dt}\vec{\omega} = \nu \nabla^2 \vec{\omega} \tag{2.44}$$

Enstrophy is defined as the square of the vorticity, so multiplying (2.44) by $\vec{\omega}$ and integrate over space yields:

$$\frac{D}{Dt} \iiint \frac{1}{2}|\vec{\omega}|^2 dV = -\nu \iiint |\nabla \times \vec{\omega}|^2 dV \tag{2.45}$$

So now we have a equation for the enstrophy, (2.45), which is used for consideration of the energy change in time when the viscosity goes to zero. The energy equation (2.25) without forcing becomes:

$$\frac{D}{Dt}E = -\nu \iiint |\vec{\omega}|^2 dV \tag{2.46}$$

In the limit $\nu \to 0$ the enstrophy will go to zero unless the triple integral of (2.45) goes like $1/\nu$. In that case the enstrophy would decrease at a constant rate, but still, from (2.46) the energy is constant

$$lim_{\nu \to 0}\frac{DE}{dt} = 0 \tag{2.47}$$

So, in two dimensional turbulence the energy is conserved when the viscosity goes to zero.

Considering (2.45) the enstrophy can not be assumed conserved in two dimensions as ν goes to zero. Therefore the assumption of $\nu = 0$ is made, which is reasonable in the inertial range. With this assumption Batchelors derivation of two directions of cascades will be followed (Batchelor, 1953).

The broadening of the energy spectrum can be expressed:

$$\frac{d}{dt} \int (\kappa - \kappa_i)^2 E d\kappa > 0 \tag{2.48}$$

where κ_i is the wavenumber where all the energy E is located initially. writing out the terms on the l.h.s. of (2.48) becomes:

$$\frac{d}{dt}(\int \kappa^2 E d\kappa - 2\kappa_i \int \kappa E d\kappa + \kappa_i^2 \int E d\kappa) > 0 \tag{2.49}$$

The first term is enstrophy which is defined as $Z = \frac{1}{2}\zeta^2$ and the third is proportional to the energy which both are conserved in time so the derivatives in time of these quantities are zero. The only contributing term is:

$$\frac{d}{dt}\left(-2\kappa_i \int \kappa E d\kappa\right) > 0 \tag{2.50}$$
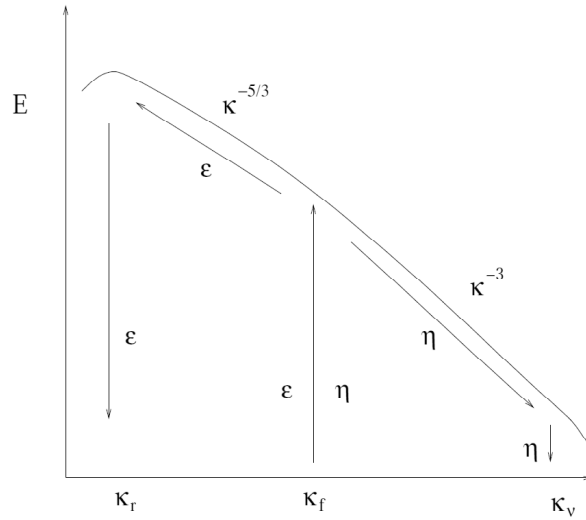
which to hold needs

$$\frac{d}{dt}\int \kappa E d\kappa < 0 \tag{2.51}$$

dividing by $\int E d\kappa$ gives the equation:

$$\frac{d}{dt}\frac{\int \kappa \int \kappa E d\kappa}{\int E d\kappa} = \frac{d}{dt}\kappa_m < 0 \tag{2.52}$$

where κ_m, the mean wavenumber is decreasing in time. This result implies a shift in the energy spectrum towards bigger scales. **Energy cascades upscale**.

Figure 2.8: *Two dimensional energy spectrum with forcing at scales k_f.* Figure by J.H. LaCasce

A similar argument is made for the enstrophy expressing its broadening of spectrum as:

$$\frac{d}{dt}\int (\kappa^2 - \kappa_i^2)^2 E d\kappa = \frac{d}{dt}\left(\int \kappa^4 E d\kappa - 2\kappa_i^2 \int \kappa^2 E d\kappa + \kappa_i^4 \int E d\kappa\right) > 0 \tag{2.53}$$

From conservation of energy and enstrophy the second and third term in (2.53) is zero, then:

$$\frac{d}{dt}\int \kappa^4 E d\kappa = \frac{d}{dt}\int \kappa^2 Z d\kappa > 0 \tag{2.54}$$

Dividing by $\int Z d\kappa$ gives the equation:

$$\frac{d}{dt}\frac{\int \kappa^2 Z d\kappa}{\int Z d\kappa} = \frac{d}{dt}\kappa_m > 0 \tag{2.55}$$

This shows a shift in the spectrum towards smaller scales. **Enstrophy cascades downscale**.

2.5.2 Inertial ranges

The inertial ranges are determined by comparing time scales. In order to find the enstrophy range, time scales for dissipation and enstrophy cascade are compared. To find the energy range, time scales for energy cascade and energy dissipation, which will be introduced later in this section, are compared.

Enstrophy range
Going back to (2.17) a time scale for dissipation can be found. Considering only the interest to find the time scale of dissipation, we focus on the first term on the l.h.s and last term on the r.h.s of (2.17). Multiplying these two terms by v:

$$v\frac{\partial}{\partial t}\vec{v} = v\nu\nabla^2\vec{v} \tag{2.56}$$

an equation for the energy change in time due to dissipation is found:

$$\frac{\partial}{\partial t}E = v\nu\nabla^2\vec{v} \tag{2.57}$$

scaling this equation:

$$\frac{V^2}{T} = \frac{V^2\nu}{L^2} \tag{2.58}$$

Then

$$T_\nu \propto \nu^{-1}k^{-2} \tag{2.59}$$

where T_ν is the dissipation time scale.

To find a time scale for the enstrophy cascade the spectrum is used. The energy spectrum of a turbulent flow in the enstrophy range can be predicted by dimension analysis. Enstrophy has units $\frac{1}{s^2}$ which gives the spectrum dimensions $1/T^2$. The flux of enstrophy η has units $1/s^3$ which gives the dimensions $1/T^3$. By dimension analysis and assuming local interaction [2] the resulting shape of the enstrophy spectrum is:

$$E(k) = C\eta^{2/3}k^{-3} \tag{2.60}$$

---

[2]Kraichnan (1970) corrected his enstrophy spectrum with a logarithmic factor, counting for non local interaction.

with a time scale for enstrophy cascade:

$$T_\eta \propto \eta^{-1/3} \tag{2.61}$$

Comparing (2.61) and (2.59) the wavelength where the transition from dissipation to enstrophy cascade takes place is found.

$$k_\eta = (\frac{\eta^{1/3}}{\nu})^{1/2} \tag{2.62}$$

At scales $k \gg k_\eta$ there is dissipation and at scales $k \ll k_\eta$ there is enstrophy cascade.

Energy range
The upscale energy cascade needs a sink at large scale to make sure the energy cascade can reach a steady state avoiding energy to pile up at larger scales. This is solved by adding a linear term to the total vorticity equation in two dimensions which represents Ekman friction. Thus from (2.43):

$$\frac{D}{Dt}\vec{\omega}_a = \nu\nabla^2\vec{\omega} - r\vec{\omega} \tag{2.63}$$

where $r = \frac{f\delta E}{2H}$ is the inverse of the Ekman spin-down time, H is the depth of the fluid and δE is the thickness of the Ekman layer. Assuming f is constant and that there are no viscous effects then:

$$\frac{D}{Dt}\vec{\omega}_a = -R\vec{\omega} \tag{2.64}$$

Solving this for t:

$$\omega(t) = \omega(0)e^{-Rt} \tag{2.65}$$

The timescale for dissipation by Ekman friction becomes:

$$T_R = R^{-1} \tag{2.66}$$

Next, the timescale for the energy flux is foun in order to compare it to (2.66). By assuming homogeneity, isotropy and only local interactions, the energy spectrum of two dimensional turbulence in the energy range only depends on the energy flux ϵ and the actual length scale. Thus, the two dimensional energy spectrum is the same as for three dimensional turbulence. To get a timescale for the energy cascade, we perform dimension analysis on (2.40) resulting in:

$$T_t \propto \epsilon^{-1/3}k^{-2/3} \tag{2.67}$$

where T_t is the timescale for the energy cascade. Comparing (2.66) and (2.67) we can determine the wavenumber where transition from Ekman damping to energy cascade occurs:

$$k_R = (\frac{R^3}{\epsilon})^{1/2} \tag{2.68}$$

At scales $k << k_R$ there is Ekman dissipation and scales $k >> k_f$ there is
an energy cascade.

Summing up, there are two interial ranges in two dimensional turbulence
theory (Kraichnan, 1967):

- **Energy inertial range**: $[k << k_{dissipation}, k >> k_{forcing}]$
  This range is above forcing scales, has a constant upscale energy flux
  and the energy spectrum $E(k) = C\epsilon^{2/3}k^{-5/3}$.

- **Enstrophy inertial range**: $[k << k_{forcing}, k >> k_{Ekman}]$ This range
  is below forcing scales constant downscale enstrophy flux and the
  energy spectrum $E(k) = C\eta^{2/3}k^{-3}$

2.5.3   Structure functions in the energy and enstrophy range

Inherent in three dimensional turbulence is Kolmogorov's four-fifths law
(2.34). To find the corresponding relation between the third order structure
function and the dissipation of energy in two dimensions, Lindborgs de-
rivation was followed (Lindborg, 1999).

Starting with the incompressible, Navier Stokes equation (2.3), adding a
driving force, $\vec{f}$ yields:

$$\frac{\partial}{\partial t}\vec{u} + \vec{u}\nabla \cdot \vec{u} = -\frac{1}{\rho}\nabla p + \nu\nabla^2\vec{u} + \vec{f} \qquad (2.69)$$

Considering velocity at a point separated by $\vec{r}$ $\vec{u}'$, in order to derive the
two point correlation function, equation 2.69 multiplied by u', is added to
equation (2.69) for u' multiplied by u. Thereafter, this sum is averaged and
under homogeneous conditions (Frisch, 1995) yields:

$$\frac{\partial}{\partial t} < \vec{u}\cdot\vec{u}' > = \frac{1}{2}\nabla\cdot < \delta\vec{u}\delta\vec{u}\cdot\delta\vec{u} > +2\nu\nabla^2 < \vec{u}\cdot\vec{u}' > + < \vec{u}\cdot\vec{f}' > +\vec{u}'\cdot\vec{f} >$$
$$(2.70)$$

where the derivatives are taken with respect to the separation vector $\vec{r}$.
Further, using the relation:

$$\nabla^2 < \vec{u}\cdot\vec{u}' > = - < \vec{\omega}\cdot\vec{\omega}' >, \qquad (2.71)$$

where $\omega = \nabla \times \vec{u}$ is the vorticity. In two dimensions, ω has only one
component perpendicular to the plane. Applying the Laplace operator on
equation (2.70) and using relation (2.71) yields:

$$-\frac{\partial}{\partial t} < \vec{\omega}\cdot\vec{\omega}' > = \frac{1}{2}\nabla^2(\nabla < \delta\vec{u}\delta\vec{u}\cdot\delta\vec{u} >) + 2\nu\nabla^4 < \vec{u}\vec{u}' > +\nabla^2 < \vec{u}\vec{f}' > +\nabla^2 < \vec{f}\vec{u}' > .$$
$$(2.72)$$

In the singel point limit, $\vec{u}' \rightarrow \vec{u}, \delta u \rightarrow 0$ and $\omega' \rightarrow \vec{\omega}$, equation (2.72) provides an equation for the enstrophy:

$$\frac{\partial}{\partial t}\Omega = -\eta + Q, \tag{2.73}$$

where $\Omega = <\vec{\omega}><\vec{\omega}>/2$ is the enstrophy,

$$\eta = \nu < \nabla\omega \cdot \nabla\omega > \tag{2.74}$$

is the enstrophy dissipation rate and

$$Q = -\nabla^2 < \vec{u} \cdot \vec{f}' > |_{r=0} \tag{2.75}$$

is the enstrophy production due to f. By combining equations (2.73) and (2.72) along with inverting the Laplacian gives:

$$\nabla \cdot < \delta\vec{u}\delta\vec{u} \cdot \delta\vec{u} >= (\epsilon_\omega - Q)r^2 + 4P - 2 < \vec{u} \cdot \vec{f}' > -2 < \vec{u}' \cdot \vec{f} > -2\nu < \delta\omega\delta\omega > \tag{2.76}$$

where

$$P = < \vec{u} \cdot \vec{f} > \tag{2.77}$$

is the energy input due to f. These equations will now be evaluated for in the enstrophy and energy range:

Enstrophy range

Assuming the forcing takes place at r_f, scales much larger than dissipation scales r_d, but smaller than the scales where Ekman dissipation takes place, equation (2.76) is evaluated:

$$Q = -\nabla^2 < \vec{u} \cdot \vec{f}' > |_{r=0} \tag{2.78}$$

is the enstrophy input due to f and

$$\epsilon_\omega = \nu < \nabla\omega \cdot \nabla\omega > \tag{2.79}$$

is the enstrophy dissipation rate, where $\omega = \nabla \times \vec{u}$ is the vorticity.

$$2\nu < \delta\omega\delta\omega > \ll \epsilon_\omega r^2 \tag{2.80}$$

due to the range being far from dissipation scales and

$$|2 < \vec{u} \cdot \vec{f}' > +2 < \vec{u}' \cdot \vec{f} > | \approx 4P - Qr^2 \tag{2.81}$$

since almost all forcing goes to production of either energy or enstrophy. Evaluating 2.76 on third terms gives:

$$\nabla < \delta\vec{u}\delta\vec{u} \cdot \delta\vec{u} >= \eta r^2 \tag{2.82}$$

Integrating and under isotropic conditions the third order structure function becomes:

$$< \delta u_L \delta u_L \delta u_L >=< \delta u_T \delta u_T \delta u_L >= \eta r^3 \tag{2.83}$$

The second order structure function can be found by dimension analysis. Assuming homogeneous, isotropic turbulence and only local interactions, the enstrophy cascade only depends on η and r:

$$< \delta u_L \delta u_L >=< \delta u_T \delta u_T >= \eta^{2/3} r^2 \qquad (2.84)$$

Energy range
Considering scales larger then r_f, but still smaller than Ekman dissipation scales gives: to hold. Simultaneously assume that

$$|(\eta - Q)r^2| \ll 4P, \qquad (2.85)$$

since there is no enstrophy production nor enstrophy dissipation at these scales, and

$$2 < \vec{u} \cdot \vec{f'} > +2 < \vec{u'} \cdot \vec{f} > \ll 4P, \qquad (2.86)$$

then, integrating (2.76) and isotropy gives the third order structure functions:

$$< \delta u_L \delta u_L \delta u_L >= 3 < \delta u_T \delta u_T \delta u_L >= \frac{3}{2} Pr \qquad (2.87)$$

The second order structure function is found by dimension analysis. Assuming homogeneous, isotropic turbulence and only local interactions, the energy cascade only depends on ϵ and r:

$$< \delta u_L \delta u_L >=< \delta u_T \delta u_T >= \epsilon^{2/3} r^{2/3} \qquad (2.88)$$

2.5.4   Isotropic relations

Isotropy is an essential assumption and has been used to find relations for energy spectra and structure functions. An estimate on the accuracy of the isotropic assumption can be carried out by calculation of two relations derived by Lindborg (1999). The first is the relation between the second order longitudonal and transverse structure functions:

$$< \delta u_T(r) \delta u_T(r)) >= \frac{d}{dr} (r < \delta u_L(r) \delta u_L(r) >) \qquad (2.89)$$

and the second the relation between the third order longitudonal and transverse structure functions:

$$< \delta u_L(r) \delta u_T(r) \delta u_T(r)) >= \frac{r}{3} \frac{d}{dr} (r < \delta u_L(r) \delta u_L(r) \delta u_L(r) >) \qquad (2.90)$$

2.6   Fluxes

Neither the spectra nor the second order structure function can determine whether there is an upscale energy cascade (two dimensional behavior) or a downscale energy flux (three dimensions behavior) in the energy range. Therefore it is necessary to measure the fluxes. The sign of the third order structure functions (2.87) can determine whether it is an upscale or downscale flux. In addition, direct flux estimates can by made by considerations of the nonlinear term in (2.3) using Fourier analysis. Next follows a derivation of the energy and enstrophy flux

Energy flux

The nonlinear term in the Navier Stokes equation give rise to redistribution of energy over the scales. Following Frisch (1995), an equation for the energy flux in spectral space will be derived.

Assumed the fluid fills all of space $\mathbf{R}^3$ and periodic boundary conditions in the space variable $\vec{r} = (x, y, z)$:

$$\vec{v}(x + nL, y + mL, z + qL) = \vec{v}(x, , y, z) \tag{2.91}$$

letting $L \to$ to ∞ implies covering the whole $\mathbf{R}^3$.
Averages over $\mathbf{R}^3$ will be notated with $<>$.

$$< f > \equiv \frac{1}{L^3} \int_{\mathbf{R}^3} f(\vec{r}) d\vec{r} \tag{2.92}$$

For periodic functions yield:

$$< \partial_i f > = 0 \tag{2.93}$$

$$< (\partial_i f) g > = - < f(\partial_i g) > \tag{2.94}$$

A low pass-filtering operator is defined

$$P_K : f(\vec{r}) \mapsto f_K^<(\vec{r}). \tag{2.95}$$

which sets all components of f with wavenumber less than K to zero. Applying P_K on (2.3) gives:

$$\frac{\partial}{\partial t} u_{i,K}^< + P_k[(u_j^< + (u_j^>)\partial_j(u_i^< + (u_i^>)] = -\nabla_i p_K^< + \nu\nabla^2 u_{i,K}^< + f_{i,K}^< \tag{2.96}$$

Multiplied by $u_{i,K}^<$ and averaged over the ensemble becomes:

$$< u_{i,K}^< \frac{\partial}{\partial t} u_{i,K}^< > + < u_{i,K}^< P_k[(u_j^< + u_j^>)\partial_j(u_i^< + u_i^>)] >$$
$$= < -u_{i,K}^< \nabla_i p_K^< > + < u_{i,K}^< \nu\nabla^2 u_{i,K}^< > + < u_{i,K}^< f_{i,K}^< > \tag{2.97}$$

Because f and p are periodic functions, from (2.93) the first and the last term on the r.h.s of (2.97) are zero and it can be written:

$$< \frac{\partial}{\partial t} \frac{|u_{i,K}^<|}{2} > + < u_{i,K}^< P_k[(u_j^< + u_j^>)\partial_j(u_i^< + u_i^>)] > = < \nu\nabla^2 u_{i,K}^< > \tag{2.98}$$

Writing out the nonlinear term:

$$< u_{i,K}^< u_{j,K}^< \partial_j u_{i,K}^< > + < u_{i,K}^< u_{j,K}^> \partial_j u_{i,K}^< >$$
$$+ < u_{i,K}^< u_{j,K}^< \partial_j u_{i,K}^> > + < u_{i,K}^< u_{j,K}^> \partial_j u_{i,K}^< > \tag{2.99}$$

These four terms are further treated one by one to determine their contribution on the energy transfer.

Using (2.93) and (2.94) on the first term in (2.99):

$$< u_{i,K}^< u_{j,K}^< \partial_j u_{i,K}^< > = - < u_{i,K}^< \partial_j (u_{j,K}^< u_{i,K}^<) > \qquad (2.100)$$

using (2.93) on the l.h.s, then yields:

$$< u_{i,K}^< u_{j,K}^< \partial_j u_{i,K}^< > = - < u_{i,K}^< u_{j,K}^< \partial_j u_{i,K}^< > \qquad (2.101)$$

which implies that this term is zero.

Following the same procedure as when finding (2.101) for the second term of (2.99):

$$< u_{i,K}^< u_{j,K}^> \partial_j u_{i,K}^< > = - < u_{i,K}^< u_{j,K}^> \partial_j u_{i,K}^< > \qquad (2.102)$$

which implies that this term is zero.

For the third term of (2.99):

$$< u_{i,K}^< u_{j,K}^< \partial_j u_{i,K}^> > = - < u_{i,K}^> u_{j,K}^< \partial_j u_{i,K}^< > \qquad (2.103)$$

which implies this term not to be zero.

For the fourth term of (2.99):

$$< u_{i,K}^< u_{j,K}^> \partial_j u_{i,K}^> > = - < u_{i,K}^> u_{j,K}^> \partial_j u_{i,K}^< > \qquad (2.104)$$

which implies this term not to be zero.

Only the last two terms of (2.99) give a contribution to the energy flux:

$$\Pi_K \equiv < u_{i,K}^< u_{j,K}^< \partial_j u_{i,K}^> > + < u_{i,K}^< u_{j,K}^> \partial_j u_{i,K}^> > \qquad (2.105)$$

where Π_K is the energy flux through wavenumber K.

Enstrophy flux

To find an equation for the energy flux, we make the same assumpitons as when we found the equation for the energy flux. Writing out the l.h.s of (2.44) we get:

$$\frac{\partial}{\partial t}\vec{\omega} + \vec{u} \cdot \nabla \vec{\omega} \qquad (2.106)$$

Considering the advecting term and multiplying this by $\vec{\omega}$ it becomes:

$$\vec{\omega}\vec{u} \cdot \nabla \vec{\omega} \qquad (2.107)$$

This equation contains the advection of enstrophy. Furthermore, dividing the components of (2.107) into highpassed and lowpassed components, the

enstrophy flux through each wavenumber is found by similar procedure as for the energy flux derivation.

$$\vec{\omega}_K{}^<(\vec{u}_K^< + \vec{u}_K^>) \cdot \nabla(\vec{\omega}_K{}^< + \vec{\omega}_K{}^>) \tag{2.108}$$

Writing out this advective term will give four terms, following the same argumentation as for (2.99) through (2.105), the enstrophy flux is:

$$\Omega_K \equiv\; < \omega_{i,K}^< u_{j,K}^< \partial_j \omega_{i,K}^> > + < \omega_{i,K}^< u_{j,K}^> \partial_j \omega_{i,K}^> > \tag{2.109}$$

The theoretical relations that were established for the velocity spectra, structure functions and fluxes will later be compared (chapter 4) to the results from the analysis of the Oleander data.

Chapter 3

Data and methods

In this chapter a description of the Oleander dataset and how it was used is presented. The chapter also presents the methods that were used to estimate the velocity spectra and structure functions. Finally, the results of testing the methods on a two dimensional model dataset with known forcing scales are presented. This is done in order to see if the results present two inertial ranges, one energy range above forcing scales and one enstrophy range below forcing scales as predicted by two dimensional turbulence theory.

3.1 Dataset
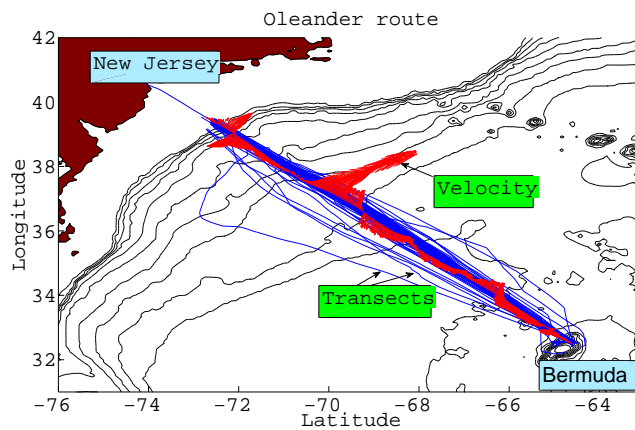
Figure 3.1: Transects (blue) for M/V Oleander in the Atlantic Ocean with the velocities (red) from one transect
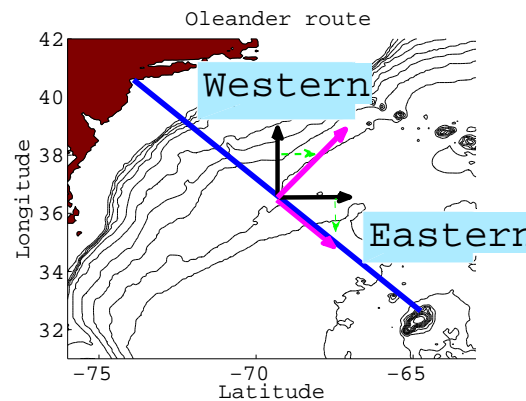
This thesis is based on a dataset from the Oleander Project. The vessel M/V Oleander operated a container service between Port Elizabeth, New Jersey and Bermuda. In the period 1994 to 2004 an acoustic Doppler current (150 kHz Teledyne RD Instruments narrowband) profiler (ADCP) mounted on

the vessel measured upper ocean velocities on its route. Absolute velocity
data were collected and averaged every 5 minutes which resulted in a spa-
tial resolution of approximately 2.4 km. The ADCP data records are avail-
able at several depths. In this study, data from depth at 55 m were analysed
aiming at illustrating the physics in the upper ocean, but also data at 155 m
and 305 m were used. More information on how ADCPs are operated on
ships can be found in Flag et.all (Flagg et al., 1998).

The dataset contains 27 different variables for each of the 421 transects re-
corded in the 10 year period. This thesis presents results based on 8 of
the variables. 6 for velocity (u (zonal) 55 m, 105 m, 305 m ,v (meridi-
onal) 55 m, 105 m, 305 m) and two for position(lattitude, longitude). To
ensure high data quality in the analysis at 55m depth, only transects with
100 percent good observations, and transect length over 1000km were used
in this study, resulting in 252 transects. For depths of 105 m, the criteria
for suitable transects were relaxed to 90 percent good observations, while
at 305m depth it was 80 percent good observations . Transect with data
sequences containing gaps larger than 8 km between observations were
discarded both at 155 m and 305 m depths. The missing data were replaced
by values obtained from interpolation over neighboring data points. This
process resulted in 256 transects at 155 m and 79 transects at 305 m.

The velocity data from the eligible
transects come as zonal and me-
ridional components.   To estab-
lish a dataset that is perpendicu-
lar and longitudinal to the tran-
sect, the grid is rotated clockwise
by an angle defined by a straight
line from New Jersey to Bermuda
and the zonal direction. This frame
rotation is necessary to calculate
the structure functions, which are
in terms of longitudinal and trans-
verse components relative to the
transect. The data points are inter-

Figure 3.2: Zonal/meridional   axis
(black)   and   longitud-
inal/transverse axis

polated onto a 2-km even grid of length 1000 km, resulting in a 500 point
grid, covering the distance from start to end for each transect. The transects
are further divided into a western region and eastern region as illustrated
in figure 3.2, this way it can be studied if the gulfstream, located in the
Western region of the transects, has an influence on the results.

Taylor's frozen turbulence hypothesis (Pope, 2000), which assumes that the
measurements at two different points are made simultaneously, is utilized.
This means that the speed of the vessel (approximately 18 knots) is much
greater than the typical speed of the disturbances. This is required for
proper interpretation of structure functions and velocity spectra.

3.2 Fourier methods

In order to apply spectral methods, one must detrend and remove the mean value of the data ensemble. These calculations along with the fast Fourier transform and linear regression, were made by applying the MATLAB software package.

3.2.1 Velocity spectra

The velocity spectra were found by treating the zonal and meridional velocities separately. First, the mean velocity and the linear trend were removed from the velocity data and interpolated onto an even grid with 2 km spacing. Then the velocity data were subject to a fast Fourier transform (FFT) in order to enter spectral space. Given the 2 km spacing in the grid, the smallest resolvable wavelengths were 4 km (two times the Nyquist frequency). The largest resolvable wavelengths were as long as the actual transect, 1000 km for the total region and 500 km for the eastern and western regions. This process was iterated for all transects. The power at each wavelength was averaged over all the transects, and the velocity spectra are presented with standard error. Linear regressions for the spectral slope were estimated in the range of wavelengths [10 km,250 km].
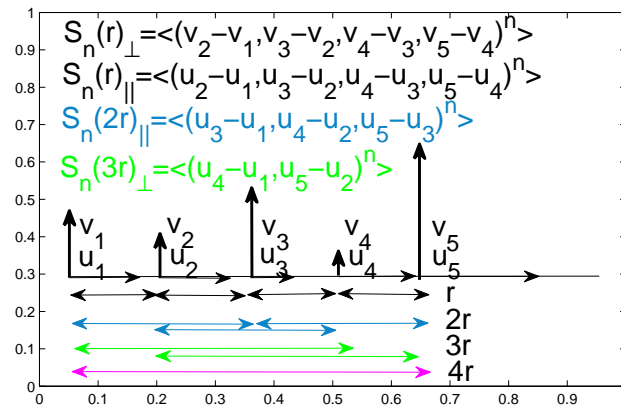
3.3 Structure functions

Figure 3.3: *Calculation of transverse (v) and longitudinal (u) structure functions.*

Following equations 2.10 and 2.11 the longitudinal and transverse second (n=2), third (n=3) and fourth (n=4) order structure functions were calculated. The gridsize of 2 km, limits the smallest separation to this magnitude, r=2 km. Then the separations were augmented to 2r, 3r, 4r and so forth,

until reaching the largest separation possible defined by the length of the grid,for the total region 1000 km and for the western and eastern regions 500 km.

In figure 3.3 it is shown how the longitudinal and transverse structure functions of order n is found.

3.4 Test of methods on model data

Next, the methods described in sections 3.2 and 3.3 will be tested on model data from a numerical simulation (LaCasce, 2010). This model simulates a two dimensional field with isotropic forcing at a short range of scales. The advantage and difference of the model data compared to the Oleander data, is that model data are two dimensional, while the Oleander data, are one dimensional. Thus, from the two dimensional model data it will be possible to estimate the energy and enstrophy fluxes directly by equations (2.105) and (2.109), and thereby see if the model presents the predicted results from two dimensional turbulence of a constant upscale energy flux and a constant downscale enstrophy flux emerging at the forced scales. In addition, this testing will show how the relations for the velocity spectra and second and third order structure functions are in regions with upscale energy or down scale enstrophy flux. If the methods present results as predicted by two dimensional turbulence theory, we can use the methods to analyse the Oleander data.

The model solves the barotropic vorticity equation with forcing and dissipation:

$$\frac{\partial}{\partial t}\xi + J(\psi,\xi) = F - D \tag{3.1}$$

where ψ is the velocity stream function, $\xi = \nabla^2\psi$ is the relative vorticity, J(,) the Jacobian function, F is an applied isotropic forcing at wavenumbers $k = [30-35]$ and D is the dissipation which was linear $-r\xi$, representing Ekman drag. In addition, an exponential cut-off filter removed enstrophy at smallest scales (LaCasce, 2002).

The Oleander data come in form of velocities. In order to get the model data to resemble the Oleander data, this thesis used the geostrophic relation to convert ψ into terms of velocity through: $u = -\frac{\partial}{\partial y}\psi$ and $v = \frac{\partial}{\partial x}\psi$.

Energy and enstrophy fluxes

Figure 3.4 presents the energy and enstrophy flux estimates. The enstrohy flux is positive (downscale) and approximately constant for k larger than

k=30-35. The energy flux is negative (upscale) for k smaller than k=30-35. This is in accordance with two dimensional turbulence theory, where there are two inertial ranges. One is a range above forcing scales, here the energy cascades upscale. And one range below forcing scale, where the enstrophy cascades downscale (chapter 2). However, the energy cascade is not constant as predicted by two dimensional turbulence theory.
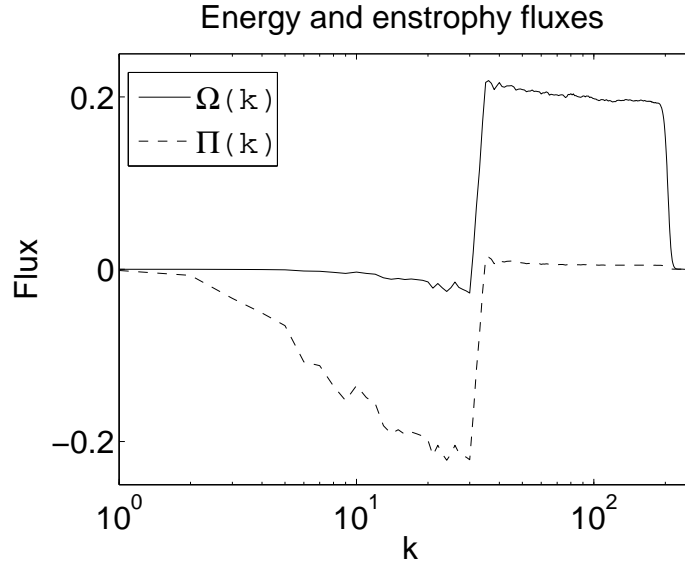

Figure 3.4: Energy (dashed) and enstrophy (solid) fluxes

Velocity spectra

Figure 3.5 (a) and (b) show the calculated velocity spectra. In (a), using a one dimensional approach, which means to consider only one line in the domain, and in (b), using a two dimensional approach, which means to use all data points in the domain. This shows that the choice of method determines the outcome. The model data are isotropic, however the one dimensional calculation shows that the transverse component holds higher energy levels than the longitudinal component. Nevertheless, this difference of the longitudonal and transverse velocity spectra is expected (Pope, 2000). On the other hand, the two dimensional approach, shows the longitudinal and transverse velocity spectra to be equal. Thus, evaluation of the energy levels of the longitudinal and transverse components in a one dimensional calculation is not appropriate to determine if the conditions are isotropic.

Even though the energy levels are not equal for the longitudonal and transverse component when estimated by the one dimensional velocity spectra method, the spectral slopes are the same for the transverse and longitudinal component. The two dimensional velocity spectra exhibit nearly identical
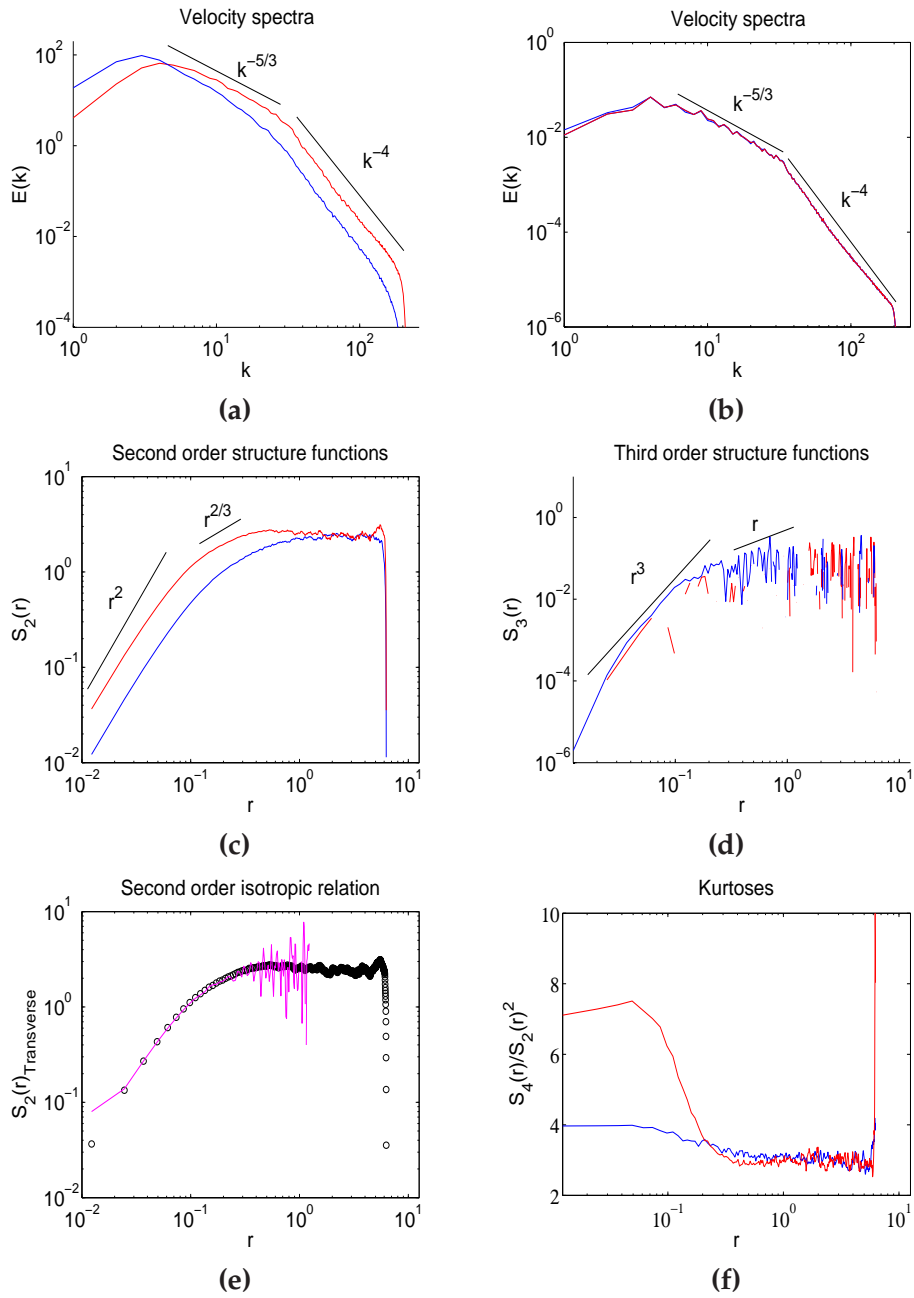
Figure 3.5: *Model data results: (a) Zonal (blue) and meridional (red) one dimensional velocity spectra. (b) Zonal (blue) and meridional (red) two dimensional velocity spectra. (c) Second order longitudinal (blue) and transverse(red) structure functions. (d) Third order longitudinal (blue) and transverse(red) structure functions. (e) Second order isotropic relation $S_2(r)_\perp$ (black dots) $\frac{d}{dr}(rS_2(r)_{||})$ (pink). (f) Kurtosis $S_4(r)/(S_2(r))^2$ (transverse(red) and longitudinal(blue))*

transverse and the longitudinal components. Considering the one dimensional and two dimensional velocity spectra, both show distinct slopes from wavelengths of k=30-35 to k=150 of k^{-4}. Kraichnans theory on two

dimensional turbulence predicted a velocity spectrum following k^{-3}. The spectral slope being steeper than the theoretical value of -3. This is explained by LaCasce with the linear dissipation acting on all scales, instead of only at larger scales, as argued for in two dimensional theory. Lacasce (2010) showed, in another simulation where the linear dissipation only acted on the larger scales, that the spectral slope was closer to -3.

In the range of wavenumbers $k = 10$ to $k = [30 - 35]$, the energy range, there are similar spectral slopes close to -5/3. This is in accordance with two dimensional turbulence theory, predicting an energy range with a velocity spectrum following $k^{-5/3}$ above forcing scales.

The Oleander data are one dimensional. Thus, only one dimensional velocity spectra were calculated.

Second and third order structure functions

In figure 3.5 (c) the estimated second order structure function is presented. In the range of separations smaller than 0.2, the zonal and meridional component show similar slopes of r^2. This is in accordance with the expected r^2 dependence predicted by the two dimensional turbulence theory for an enstrophy cascade. Forcing at k=30-35, corresponds to separations of r=0.18-0.21 ($\frac{2\pi}{35} - \frac{2\pi}{30}$). For separations greater than 0.2, a constant slope is not clearly found. It seems like curve is rolling off the r^2 dependence. It can be argued that a $r^{2/3}$ dependence is recognized, but this is for less than a decade of wavenumbers. In addition, any tangent to the curve will fit at some point, thus the $r^{2/3}$ dependence does not clearly stand out.

Figure 3.5 (d) shows the third order structure function. The result appears to be inconclusive for the transverse component for smaller separations. The longitudinal seems to have a r^3 dependence in accordance with two dimensional turbulence theory for an enstrophy cascade. For larger separations, the results appear inconclusive for both components althogh they flatten out.

In the enstrophy range, the second order structure functions reproduce the expected results according to two dimensional turbulence theory. However, the value of the energy spectra is k^{-4}. The reason for this is that all spectra with a steeper slope than -3 will present a r^2 dependence of the second order structure function (LaCasce, 2008)(Bennet, 1984).

On the other hand, the third order structure function are very noisy, especially at larger separations where there are less data, and can suggest poor statistical convergence (LaCasce, 2002). Also, the third order structure function beeing of uneven power, can invoke negative values. Thus, the expected results are only recognized to some extent. However, prior

analysis in the field (Lindborg, 1999) used third order structure functions with success. Therefore, both second and third order structure functions were calculated, although the third order structure functions were noisy.

Second order isotropic relation and kurtosis

In figure 3.5 (d) and (e) the second order isotropic relation and the kurtosis is illustrated. The first shows good accordance up to separations of 0.4, indicating isotropy. This is as expected from the two dimensional velocity spectra, and also from the model which is set up on the f-plane with isotropic forcing, so the statistics must be isotropic. The kurtosis is also quite smooth and constant, for the longitudonal component. On the other hand, the transverse kurtosis has larger values, and is increasing for smaller separations. This could explain the poor result of the third order structure function.

Conclusions from testing the methods

Flux calculations revealed a nearly constant downscale enstrophy flux below forcing scales. In this range, the results from testing the methods on the two dimensional model data have shown that the velocity spectra and second and third order structure functions followed the predicted relations by two dimensional turbulence theory in the enstrophy inertial range.

In the energy inertial, there is an upscale cascade. Even though this upscale cascade is not constant as predicted by the two dimensional theory, it is present. In addition, the velocity spectra show the predicted $k^{-5/3}$ dependence. However, the second order structure functions do not show a clear $r^{2/3}$ dependence. This means that, perhaps, the second order structure function could not miss the presence of an upscale energy flux. The third order structure functions in this range gave no conclusive results.

Chapter 4

Results

This chapter presents results derived by applying the methods described in chapter 3 on the Oleander data. They are presented in two rounds. First from the records extracted at 55 m depth, then together for the records extracted at 155 m and 305 m depths. Within these two rounds, the results are presented by method, starting with the second order isotropic relation, aiming to validate isotropic conditions, a fundamental assumption in two dimensional turbulence theory. Then, velocity spectra, second and third order structure functions are illustrated and compared to the expected relations from two dimensional turbulence theory. The velocity spectra were also estimated for different subsets at different times, this to evaluate stationarity. Thereafter, the kurtoses, which is intended to detect intermittency are presented. The conversion between wavelenghts and eddyscales are straight forward. In this thesis a ratio of 4:1.has been assumed (4 km wavelenght : 1 km eddy scale).

4.1 Analysis at 55 m depth

The results are focused on the longitudinal/transverse components in order to have the same base for calculations of velocity spectra and structure functions. This is different from Wang et al. (2010) who used zonal/meridional components in their analysis.

4.1.1 Test for isotropy

In figure 4.1, the transverse second order structure functions are presented. At separations up to 40km, all regions show good accordance between the directly calculated transverse component and the transverse component calculated from the isotropic relation (2.89). At larger separations (scales larger than 40 km), all regions exhibit the same tendency of a fluctuating isotropic relation curve, which could be explained by less data at the larger scales. However, it could be argued that the eastern region holds good
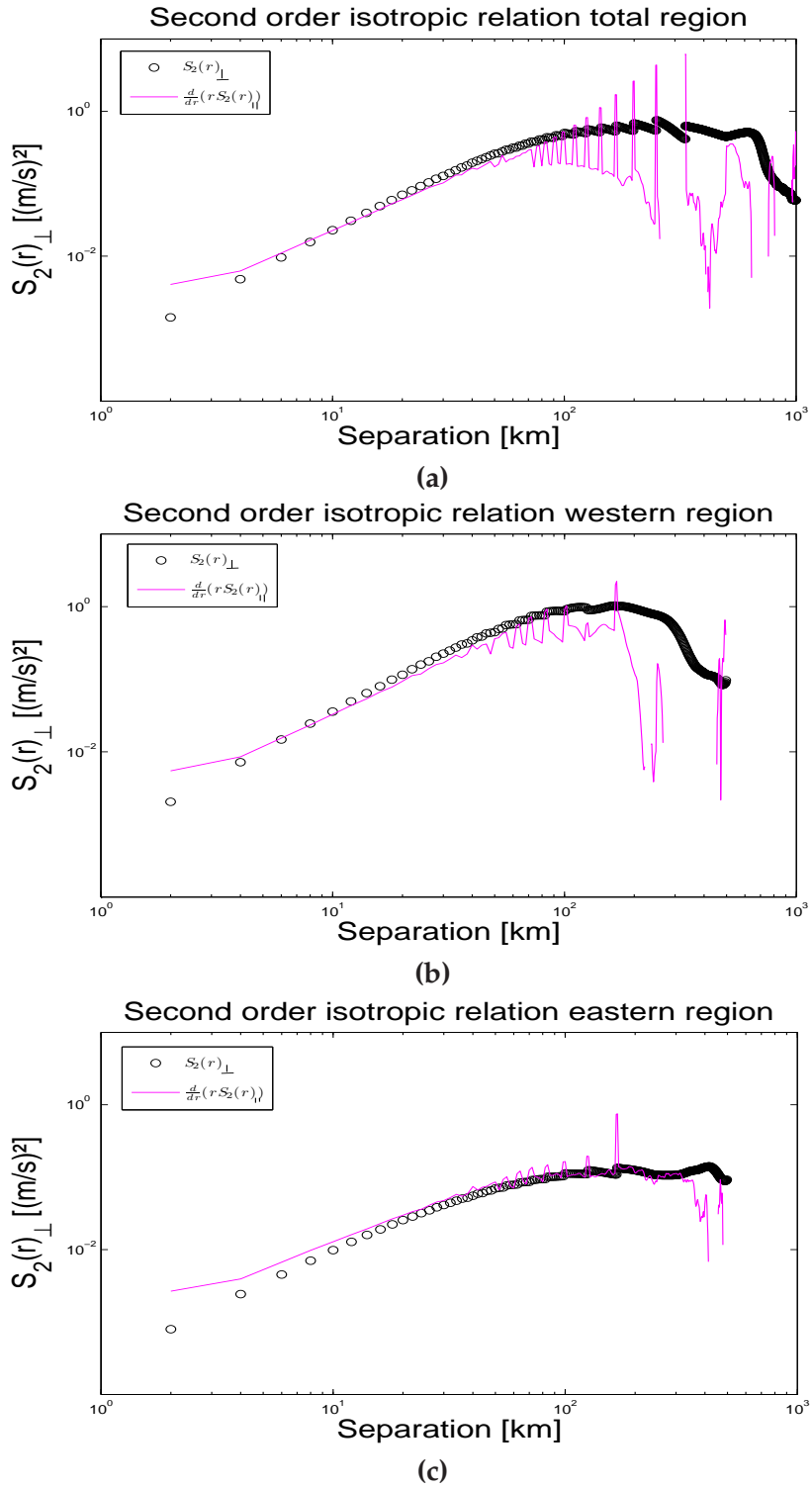
Figure 4.1: *Transverse second order structure function calculated directly(black dotted) and from the isotropic relation(pink) for the total(a), western(b) and eastern(c) regions.*

accordance with the relation for separations up to 120 km. Thus, the assumption of isotropy is accurate at scales smaller than 40km in all regions and to some extent for scales up to 120 km in the eastern region.
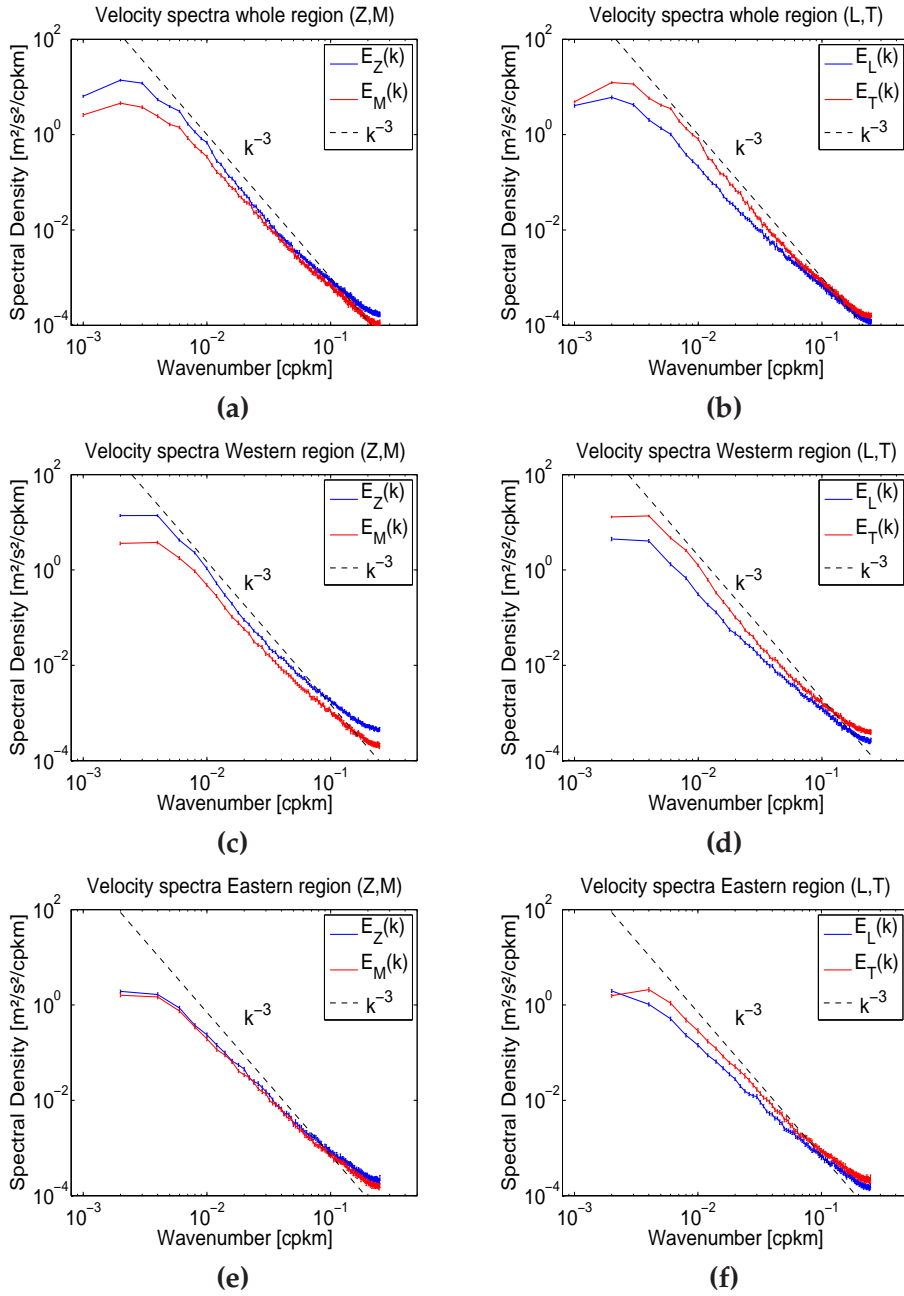
4.1.2   Velocity spectra

Figure 4.2 illustrates the estimated one dimensional velocity spectra for the region of measurements at 55 m and two subsets,the eastern and western regions. The left panel illustrates the zonal and meridional components, while the right panel illustrates the transverse and longitudinal components. All the velocity spectra are presented with errorbars indicating the standarderror and the theoretical k^{-3} velocity spectra expected in an enstrophy cascade range.

All regions exhibit velocity spectra with distinct linear slopes in the range of wavelengths 10-250 km. A top in the spectra is recognizable at approximately 300km wavelength, invoking the largest energy. The zonal/meridional and longitudinal/transverse linear slopes are reasonably equal, in particular for the eastern region, and thereby suggests isotropy within the regions. Thus, these results are consistent with the second order isotropic relation results at smaller scales.

The total and western regions exhibit spectral slopes very close to -3. The eastern region exhibits slightly less steep spectral slopes at the larger scales, but is still close to -3 in the range of wavelengths 10-250 km. This is in good accordance with the velocity spectra $E(k) \propto k^{-3}$ corresponding to an enstrophy cascade in two dimensional turbulence theory. None of the regions show sign of a slope of -5/3 . The absence of a velocity spectra with a $k^{-5/3}$ dependence over longer range will be discussed in chapter 5.

Studying the longitudinal/transverse velocity spectra (Right panel of figure 4.2), they show the transverse component to contain larger energy. This is in accordance with the results from velocity spectra calculations performed on the model data in section 3.4. On the other hand, the zonal/meridional analyzed by Wang et al. (2010) components seem to have reasonable equipartition for the measured directions. These results concern istropy and will be discussed in chapter 5.

Figure 4.2: *(Left)Zonal (blue) and meridional (red) velocity spectra in (a) (total region), (c) (western region) and (e) (eastern transect). (Right) Transverse(red) and longitudinal (blue) velocity spectra in (b) (total region), (d) (western region) and (f) (eastern region) . Standarderror is marked.*
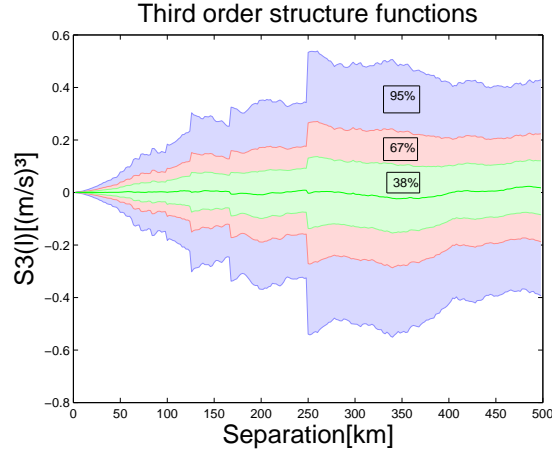
4.1.3   Structure functions

The variability in the calculated structure functions are huge, whether these are calculated for one transect or over the all transects. Therefore, the structure functions in this thesis are presented without errorbars for a clearer presentation of the results.

To illustrate the variability in the structure functions, figure 4.1.3 and
4.1.3 show different confidence intervals for the second and third order
longitudinal structure function in the eastern region.
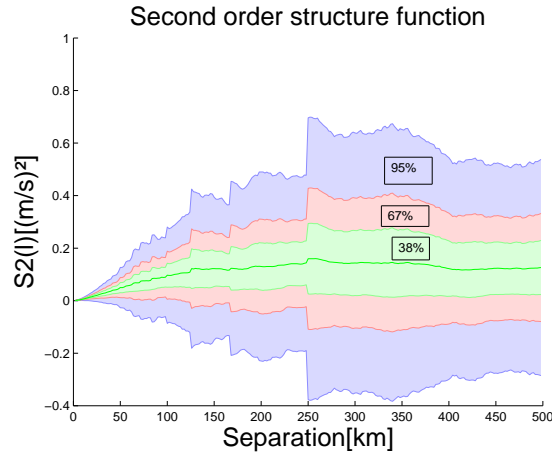
Figure 4.3: *Second order longitudinal structure functions versus separation distance from
Oleander data for the eastern region of measurements.*

Figure 4.4: *Third order longitudinal structure functions versus separation distance from
Oleander data for the eastern region of measurements.*

Second order structure functions

In figures 4.5 (a), (b) and (c), the longitudinal and transverse second order structure functions at 55 m for the total, western and eastern regions are plotted in a log-log plot. The black lines are the expected separation dependencies in two dimensional turbulence theory of an energy range following a power-law dependence of $r^{2/3}$ and the enstrophy range following a power-law dependence of r^2.

All regions exhibit a power-law dependence in the range of separations [2-40 km]. In this range, the total and western regions exhibit a close r^2 dependence. The eastern region exhibits slightly less steeper curves, apparently rolling of the r^2 dependence at smaller separations than the other two regions, but still holds a reasonably close r^2 dependence. The transverse and longitudinal curves exhibit reasonably similar power-laws. These results are in accordance with the theoretical relations expected in an enstrophy range in two dimensional turbulence. They are also consistent with the velocity spectra results at these scales.

In the range of separations [40-120 km] all regions have curves that roll off a steeper power-law dependence. Thus, there are no distinct ranges in any regions showing a power-law dependence of $r^{2/3}$. These results are consistent with the velocity spectra.

Third order structure functions

In figure 4.6 the longitudinal and transverse third order structure functions for the longitudinal and transverse velocities are presented. The black lines are the predicted power-law (r^3) which corresponds to an enstrophy cascade and the linear curve r which corresponds to an energy cascade according to two dimensional turbulence theory. Noticeable is the disparity of the eastern region compared to the the western and total region.

Western and total region
Considering the western and total regions for separations in the range [2-40 km], they exhibit distinct power-law dependencies close to r^3. Also, the third order structure functions are positive in this range. These results are in accordance with an enstrophy cascade in two dimensional turbulence theory.

(a)

(b)

(c)
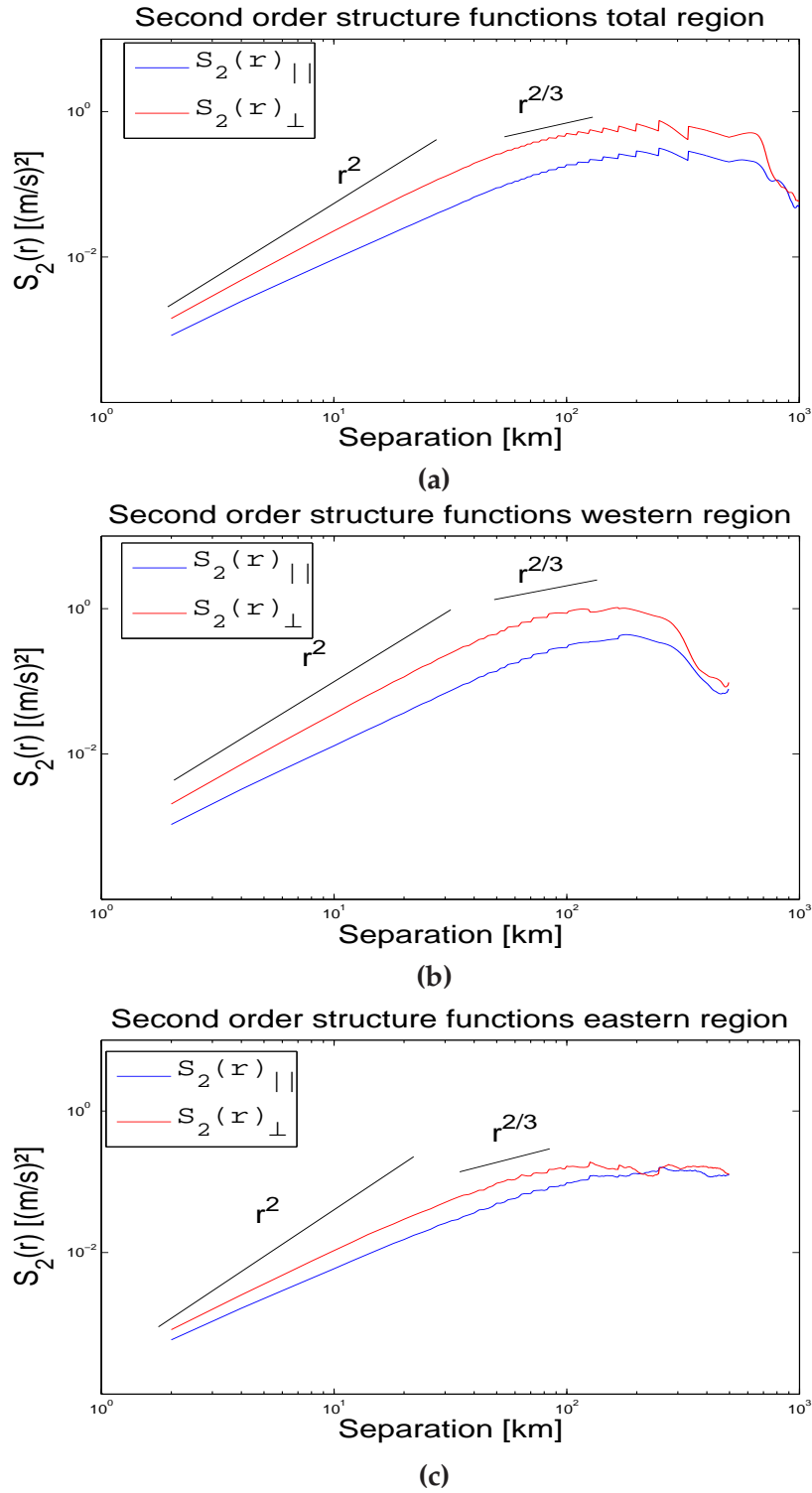
Figure 4.5: *Second order longitudinal(blue) and transverse(red) structure functions versus separation distance from Oleander data at 55m depth for the (a) total, (b) western and (c) eastern region of the transect. The black lines are theoretical separation dependencies $r^{2/3}$ (energy) and r^2 (enstrophy) from two dimensional turbulence theory.*

On the other hand, the transverse and longitudinal third order structure functions are not equal. This indicates anisotropic conditions. Thus, these results are not consistent with the results from the second order isotropic relation and will be discussed in chapter 5.
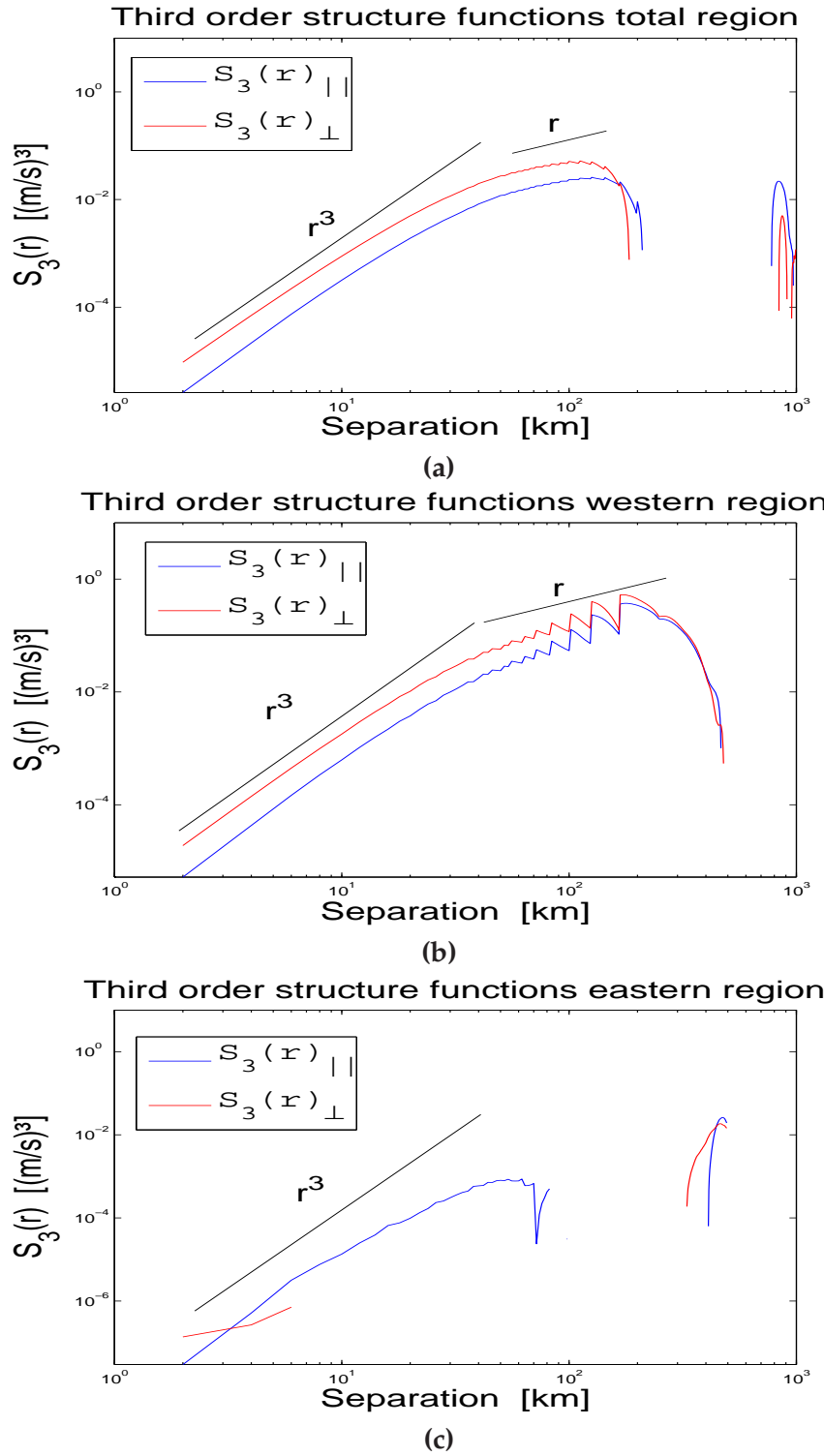
Eastern region

Considering the range of separations [2-40 km], the results obtained from the eastern region of measurements are distinctly different from the other two regions. First, the transverse component is negative, which from equation (2.83), suggests an upscale enstrophy flux. This result is not in accordance with two dimensional turbulence and will be discussed in chapter 5. Second, the longitudinal arguably shows a power-law dependence of r^3. These results are not in accordance with two dimensional turbulence theory as prior results were at these smaller scales, and will be discussed in chapter 5.
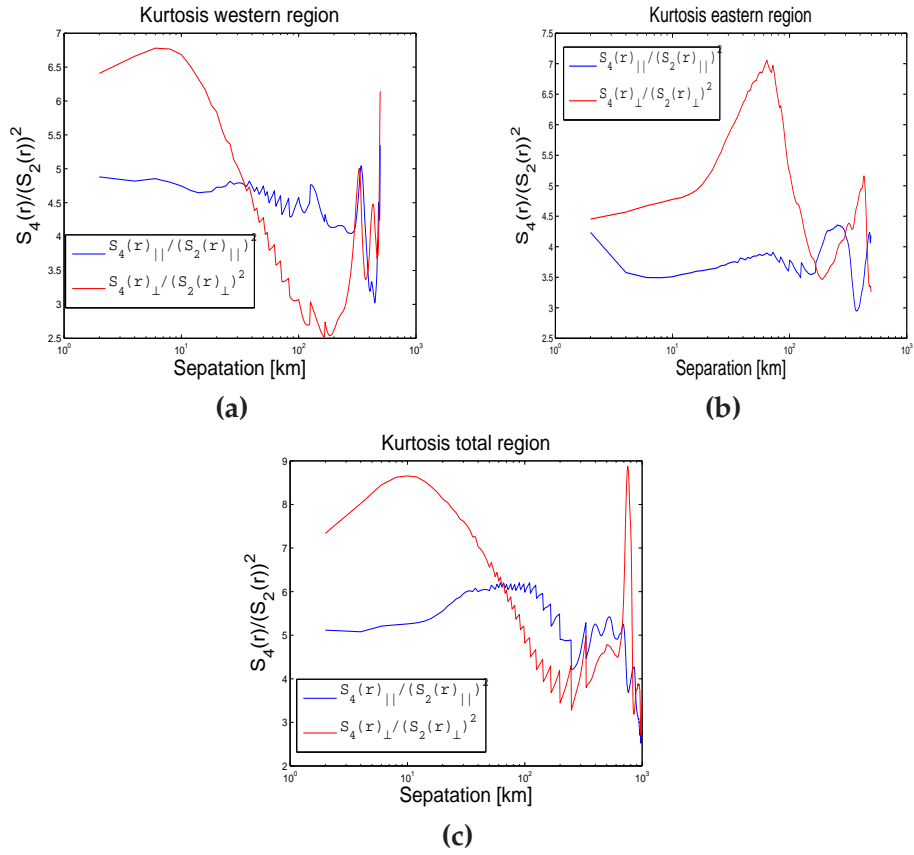
Kurtoses

Figure 4.7 illustrates the kurtoses for the transverse and longitudinal velocity component in the western, eastern and total regions. The transverse component is generally higher for smaller separations. However, the eastern region kurtosis curve includes a peak at intermediate separations of approximately 80km. The longitudinal component contains similar values at all separations in all regions.

For most separations the kurtosis value is larger than three. Thus, the velocities do not have a Gaussian distribution, indicating presence of some relatively rare but high-amplitude events. This could be an issue considering that the velocity spectra were presented with standard error which strictly is to be used for Gaussian distributions. This issue will be discussed in chapter 5.

Figure 4.6: *Third order longitudinal(blue) and transverse(red) structure functions versus separation distance from Oleander data at 55 m depth for the (a) total, (b) western and (c) eastern region of the transect. The black lines are theoretical separation dependencies r (energy) and r^3 (enstrophy) from two dimensional turbulence theory.*

Figure 4.7: *Kurtosis factor for longitudinal(blue) and transverse(red) velocities in the western region (a), eastern region(b) and total region (c) of measurements.*

4.2 Analysis at 155 m and 305 m depths

This section contains the results obtained from applying the same methods as in the 55 m depth analysis at 155 m and 305 m depth data. They are presented in the same order as for the 55 m results, starting with the second order isotropic relation. In all figures the 155 m results will be in the left panel, while the 305 m results will be in the right panel. Comparing results from various depths will suggest if the turbulent dynamics are independent of depth.
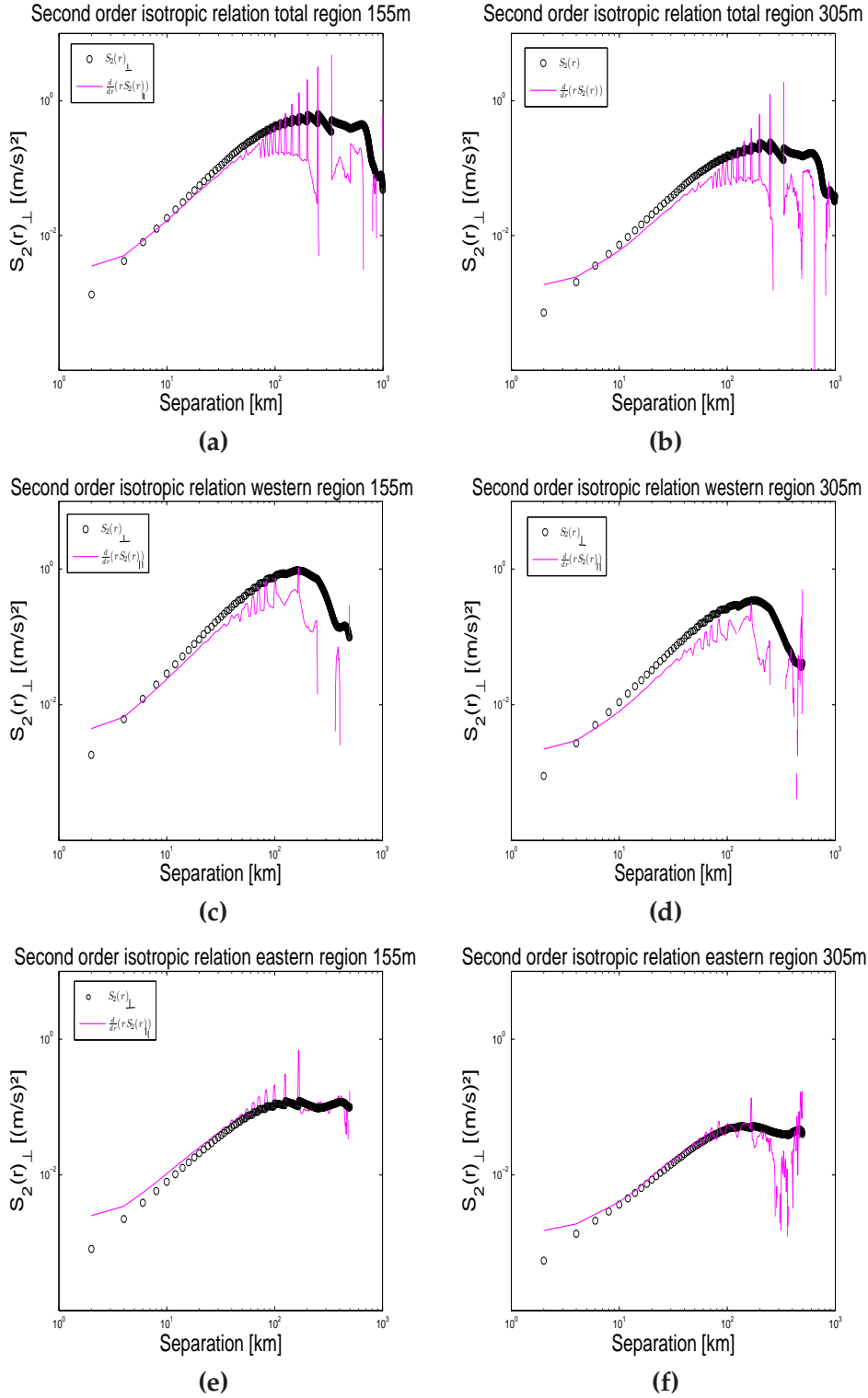
4.2.1 Second order isotropic relation

The isotropic relation is held for separations up to 40 km, both at 155 m (figure 4.8, left panel) and 305m (figure 4.8, right panel) depths in all regions. At separations larger than 40km the isotropic relation curves are very noisy and show anisotropic behavior. Noticeably, the eastern region holds for larger scales than the western and total regions. These results are consistent with the results at 55 m for separations smaller than 40 km and also consistent regarding the eastern region holding the isotropic relation up to larger scales than the other regions.
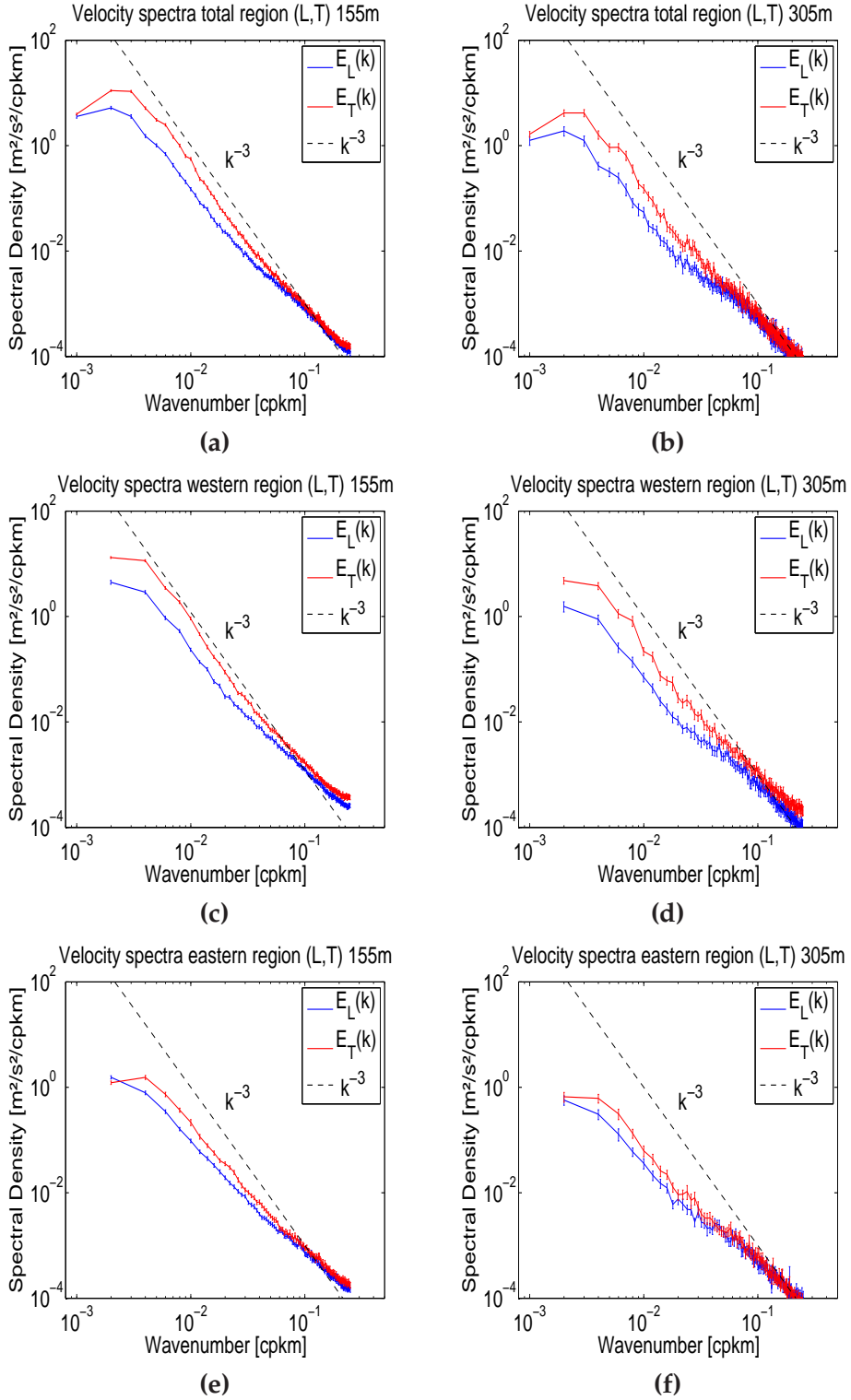
4.2.2 Velocity spectra

The longitudinal and transverse velocity spectra at 155m depth are presented in the left panel of figure 4.9. The total and western regions show power-law dependencies close to k^{-3} in the range [10,250 km] wavelengths. Considering the eastern region, the results also shows power-law dependence in the range [10,150 km], however there is an offset at approximately 30km wavelengths.

At 305 m depth, right panel of figure 4.9, the spectral slopes are less constant. The curves are not smooth, however, the regions do to some extend exhibit k^{-3} dependencies.

The results are consistent with 55 m results, even though the 305 m results had noisy curves. This will be discussed in chapter 5.

(a)

(b)

(c)

(d)

(e)

(f)

Figure 4.8: *Transverse second order structure function calculated directly (black dotted) and from the isotropic relation (pink) at 155 m (left) in a (total region), c (western region) and e (eastern transect) and at 305 m (right) in b (total transect), d (western region) and f (eastern region).*

Figure 4.9: *longitudinal (blue) and transverse (red) velocity spectra at 155 m (left) in a (total region), c (western region) and e (eastern transect) and at 305 m (right) in b (total transect), d (western region) and f (eastern region). Standarderror is marked.*

4.2.3   Structure functions

Second order structure functions

In figure 4.10 the second order structure functions at 155 m (left panel) and
305 m (right panel) are presented. Considering the range of separations
[2-40 km], the slopes on the curves are reasonably constant with increased
depth within each region. The total and western regions at 155 m and 305
m indicate a reasonable r^2 dependence, while the eastern region only holds
an r^2 dependence below 10 km scales, for larger scales the curve start to roll
off. This is consistent with the velocity spectra, showing the eastern region
to invoke the flatter curves.

Considering separations larger than 40 km, both the 155 m and 305 m
results show the same tendency of curves rolling from a steeper to more
moderate slope.

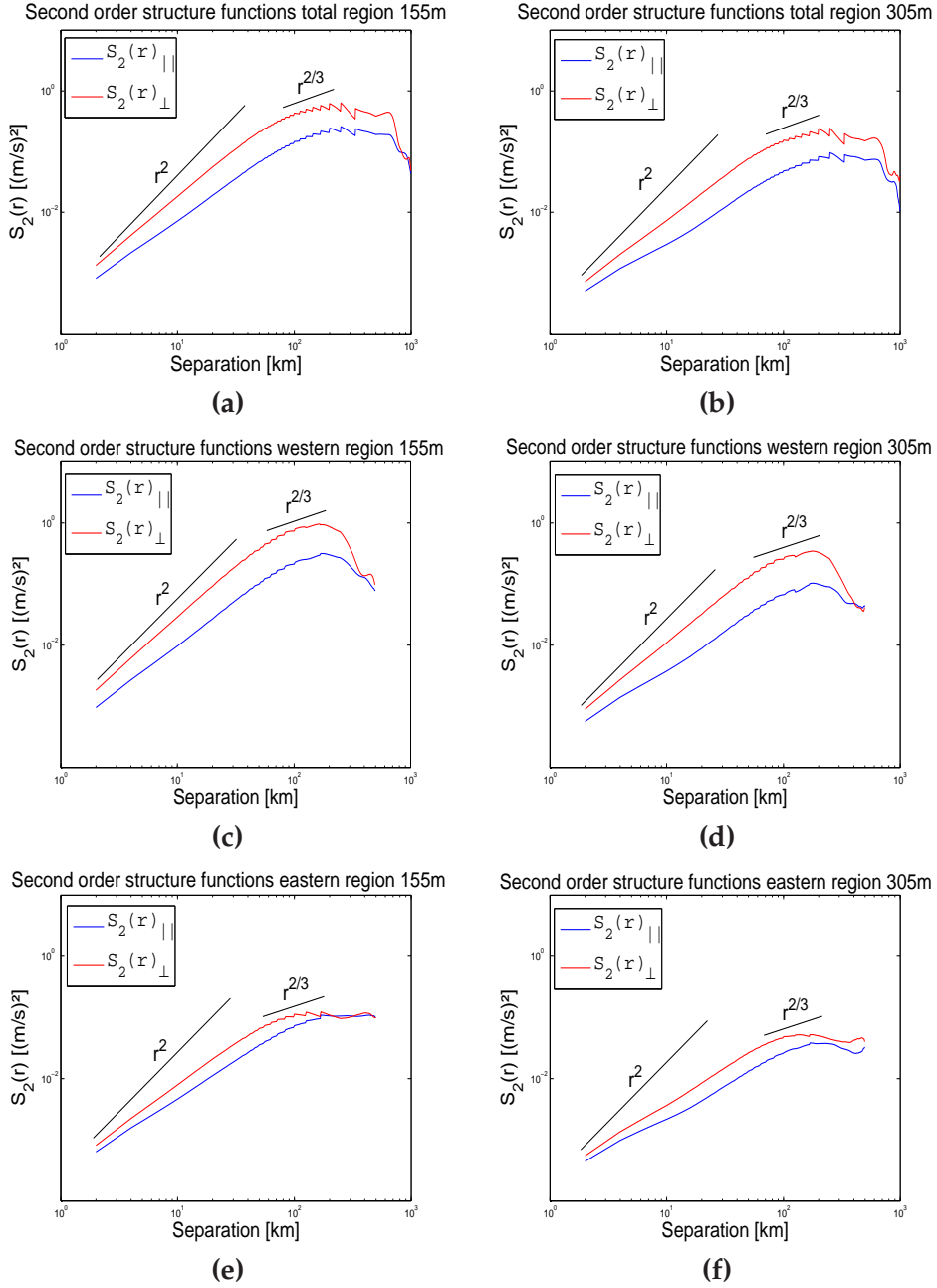**Third order structure functions**

In figure 4.11 the longitudinal and transverse third order structure func-
tions at 155 m (left) and 305m(right) are presented. Recalling the results
of these measures from 55 m records, also at 155 m and 305 m, the eastern
region presents clearly different results than the western and total regions.
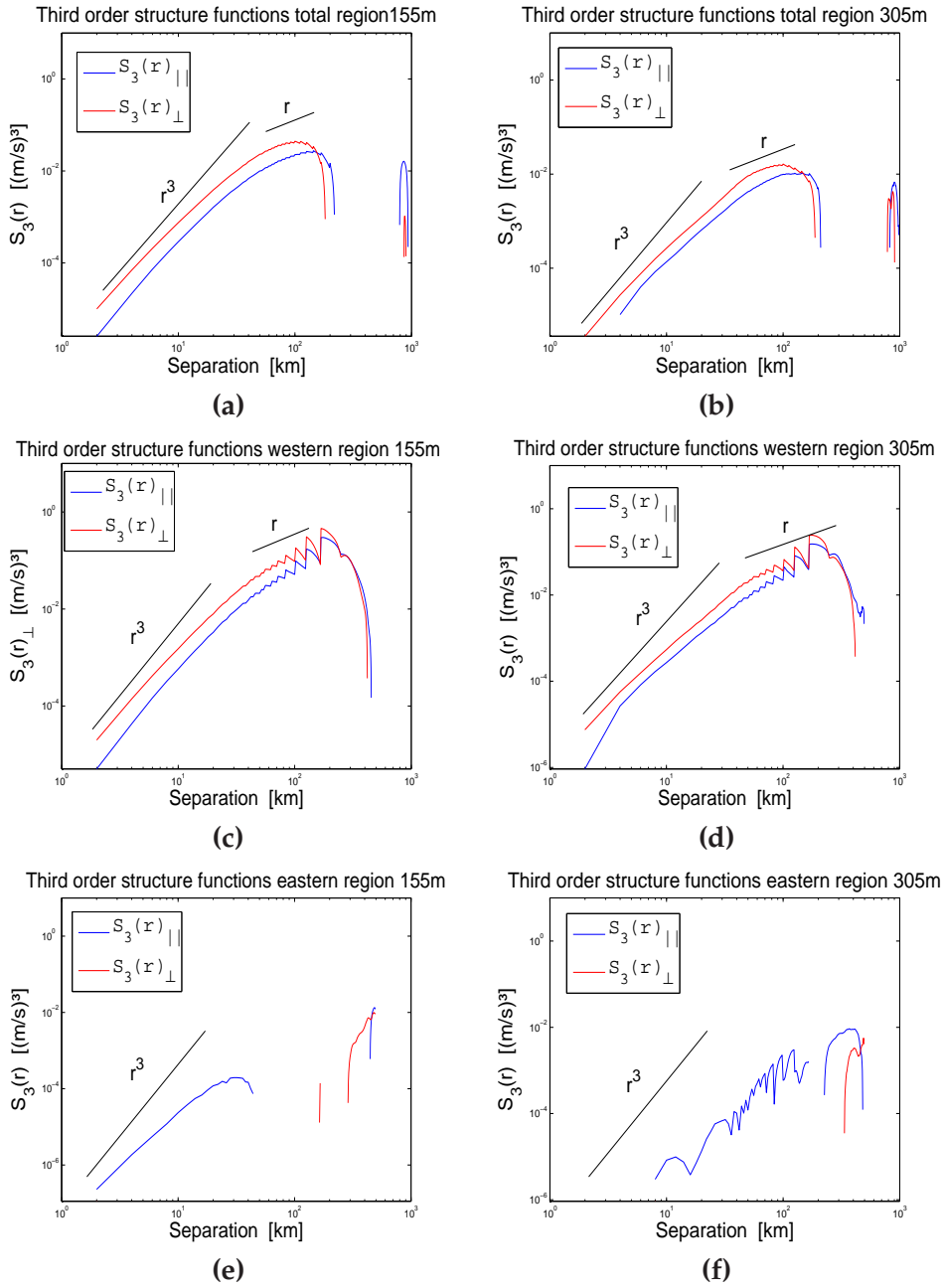
Western and total regions
Considering the results from 155 m in the range of separations [2-40 km],
the total and western regions show reasonable r^3 dependencies and are
positive. The 305 m results are similar, but start to level at smaller separ-
ations. At 155m and 305 m depths as the shallower depth, the longitud-
inal and the transverse components are different. However, the difference
between the curves seems more like an offset. Without the offset, the two
curves would be very similar. This observation will be discussed in chapter
5.

Eastern region
The results are similar to those obtained from 55 m records with the
transverse components being positive. At 155 m depth the longitudinal
component follows a reasonable r^3 dependence, however it rolls off at
smaller scales compared to the 55 m depth result. In addition, the
longitudinal component at 305 m depth presents very noisy results and
is of arguable r^3 dependence.

Figure 4.10: *Second order Longitudinal (blue) and transverse (red) structure functions versus separation distance at 155 m (left) for the (a) total, (c) western and (e) and at 305 m (right) for the (b) total, (d) western and (f) eastern region of measurements.*

Figure 4.11: *Third order Longitudinal(blue) and transverse(red) structure functions versus separation distance at 155 m (left) for the (a) total, (c) western and (e) and at 305 m (right) for the (b) total, (d) western and (f) eastern region of the transect.*

Kurtoses

The results of the kurtosis curves at 155 m (left panel) and at 305 m (right panel) exhibit similar shapes and values as the 55 m kurtosis curves 4.7. The values are mostly larger than 3 in all regions, which means there are

intermittecy effects present at all depths. This could affect the higher order statisctics. The results are consistent with the second and third order structure and velocity spectra showing similar relations at the three depths.

Figure 4.12: *Longitudinal (blue) and transverse (red) kurtoses at 155 m (left) for the (a) total, (c) western and (e) and at 305 m (right) for the (b) total, (d) western and (f) eastern region of the transect.*
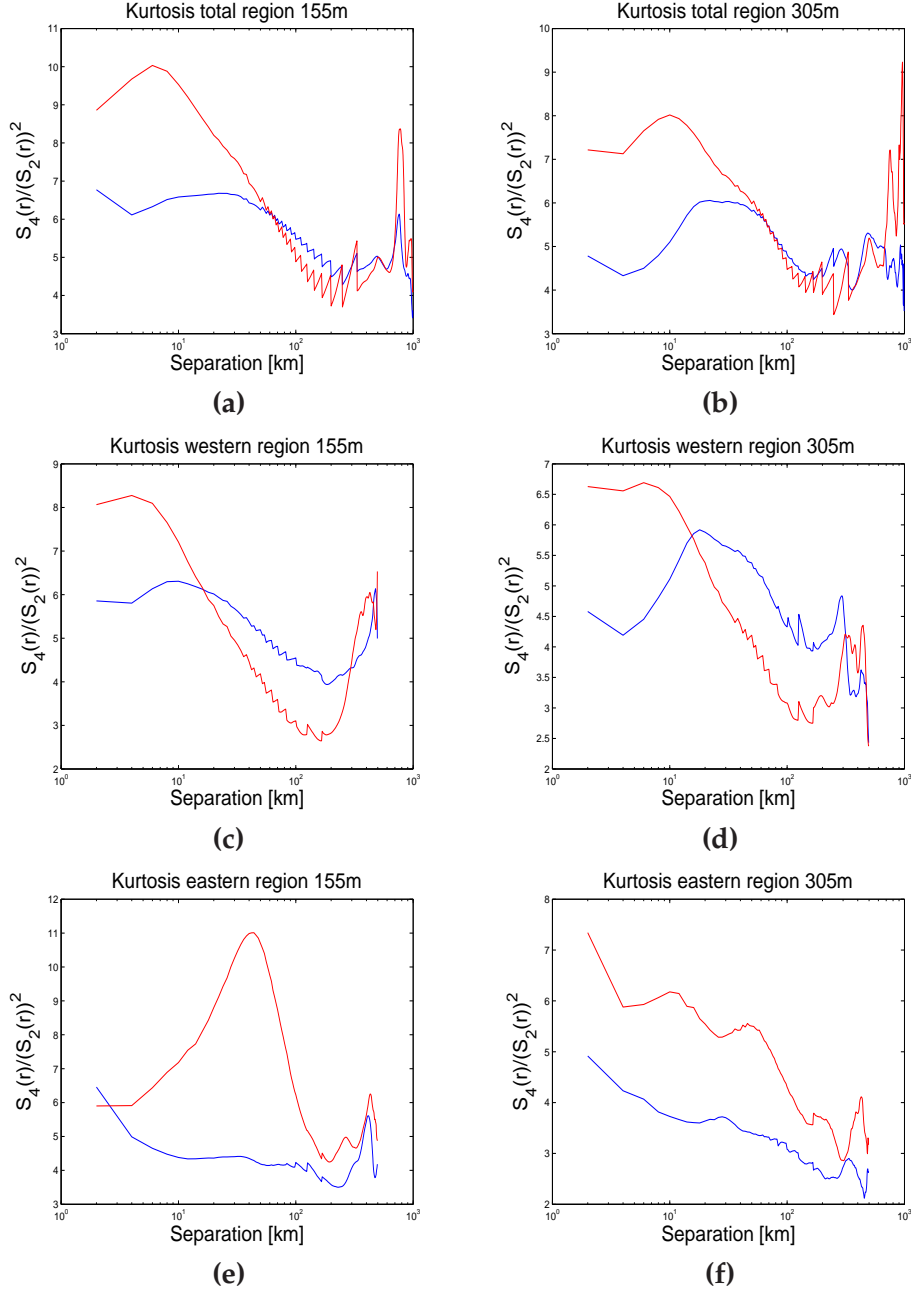
Chapter 5

Discussion

The response of the Oleander dataset to the applied methods is all in all apparently in good agreement with two dimensional turbulence theory. In this chapter however, incompatible results , and factors that may have an impact on the interpretation of the results, are discussed.

5.1   Assumptions

Performing analysis on data from real measurements is very different from performing analysis on data retrieved from numerical simulations. For the Oleander data, the assumptions can not be expected to be perfectly held, but the grade of violation and consequences must be considered.

Isotropy

To test the assumption of isotropy, the second order isotropic relation was applied at the Oleander data. The noisy curve of the isotropic relation at larger scales could be caused by less data at these larger scales, and not by anisotropy. Thereby, conditions may also be isotropic at scales larger than approximately 40 km. However, isotropic conditions at larger scales will not break isotropy at scales below 40 km. Two dimensional turbulence assumes local isotropy, so if the break of the isotropic relation at larger scales actually is from anisotropy, this does not constitute a problem for the theory.

Considering the velocity spectra of the western and eastern region at 55 m depth, the latter exhibits practically identical spectral slopes in both the longitudinal and transverse direction. The western region, however, exhibits moderate differences in the spectral slopes at larger scales. This is in accordance with the second order isotropic relation, holding better in the eastern region. The moderate break of isotropy in the western region,

could be explained by the Gulf Stream located in the western region. The Gulf Stream's direction is more aligned with the transverse direction, therefore, there is more energy in the transverse component. Another factor could be the bottom topography, whose contour lines, illustrated in figure 3.2, support greater velocities in the transverse direction. These factors were acknowledged, but considered not to be an issue since they are mainly present at larger scales.

The third order structure functions do to some extent exhibit anisotropy. Following two dimensional turbulence theory, the third order transverse and longitudinal structure functions should be equal under isotropic conditions (equation 2.90). The Oleander data results show they are not, particularly in the eastern region. This is in contrast with the second order structure functions, which exhibited the most isotropic results in the eastern region. However, if the results from the eastern regions are overlooked, it is observed that the longitudinal and transverse third order structure functions, at all depths, are similar and only separated by an offset. So the results are not completely off. The kurtosis showed intermittency effects. This will have an impact on the third order structure functions by limiting its statistical convergence. Thereby, we get the disparity between the third order structure function results and the second order isotropic relation results. So from these arguments, the results of the second order structure functions exhibiting istropy are not falsified.

Homogeneity

In figure 5.1, the left panel illustrates the longitudinal components and the right panel illustrates the transverse components of velocity spectra and second and third order structure functions. Considering the velocity spectra by component, the three regions show different energy levels at wavelengths larger than approximately 80 km, more so the transverse components. This could be explained by the Gulf Stream injecting more energy into the transverse component at these wavelengths. At scales below approximately 100 km wavelengths, the velocity spectra in the same direction of the three regions are comparable, particularly the total and eastern regions. This result suggests arguable homogenic conditions at wavelengths below approximately 100 km (25 km scales).

The observation of different energy levels at the same wavenumber k, suggest that the energy flux at the scales corresponding to k, is not the same in all regions. Thus, the energy flux is not the same everywhere, and finding e.g energy spectra by dimensional analysis assuming that they only depend on the energy flux and the actual length scale is not accurate. This is known as Landau's objection (Frisch, 1995).

When evaluating the second order structure functions, it is seen that they
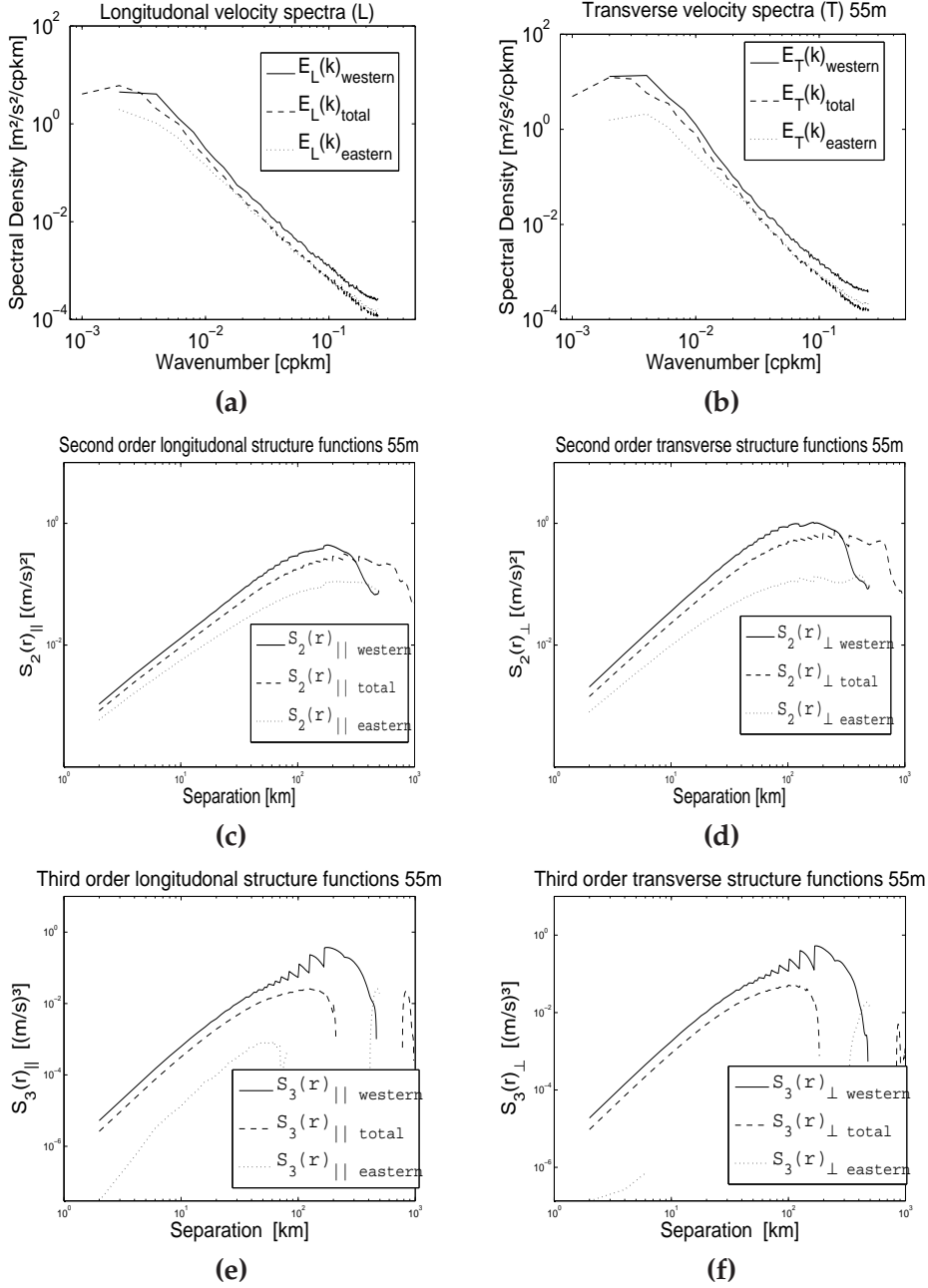
Figure 5.1: *Longitudinal (left panel) and transverse (right panel) velocity spectra (a) (b), second (c) (d) and third (e) (f) structure functions for the western (solid), total (dashed) and eastern (dotted) region of measurements.*

are dependent on the region of measurement, particularly the transverse component, which is consistent with the velocity spectra. However, the longitudinal components show the same slopes below around 40 km scales and the transverse components for around 25 km scales. The distinct power-law dependencies suggest that turbulence is present in all regions and fills the whole space. This makes it homogenic in the sense all regions invoke turbulence. Nevertheless, the dependence of region indicates that

it is not completely homogenic, but that there are some sort of local ho-
mogenic conditions within each region. Because of the uncertainty in the
structure functions (figure 4.1.3), it is difficult to evaluate the grade of dif-
ferences between the structure functions in the regions. The differences
with region are not considered as determining. Thus, homogenic condi-
tions arguably exist below 40 km scales.

The third order structure functions at scales below 40 km in the eastern
region are noticeably different compared to the third order structure
functions in the western and total regions, specially the transverse
component. However, the longitudinal component in the eastern region
seems to roll off a steeper power-law. This is consistent with the two other
regions. On the other hand, the transverse component, being positive,
is very different. This result could break the assumption of homogenic
conditions.   However, following the arguments of the poor statistical
convergence for higher order statistics, these results are not considered
as accurate in determining if conditions are homogenic. Considering the

(a)

(b)

(c)
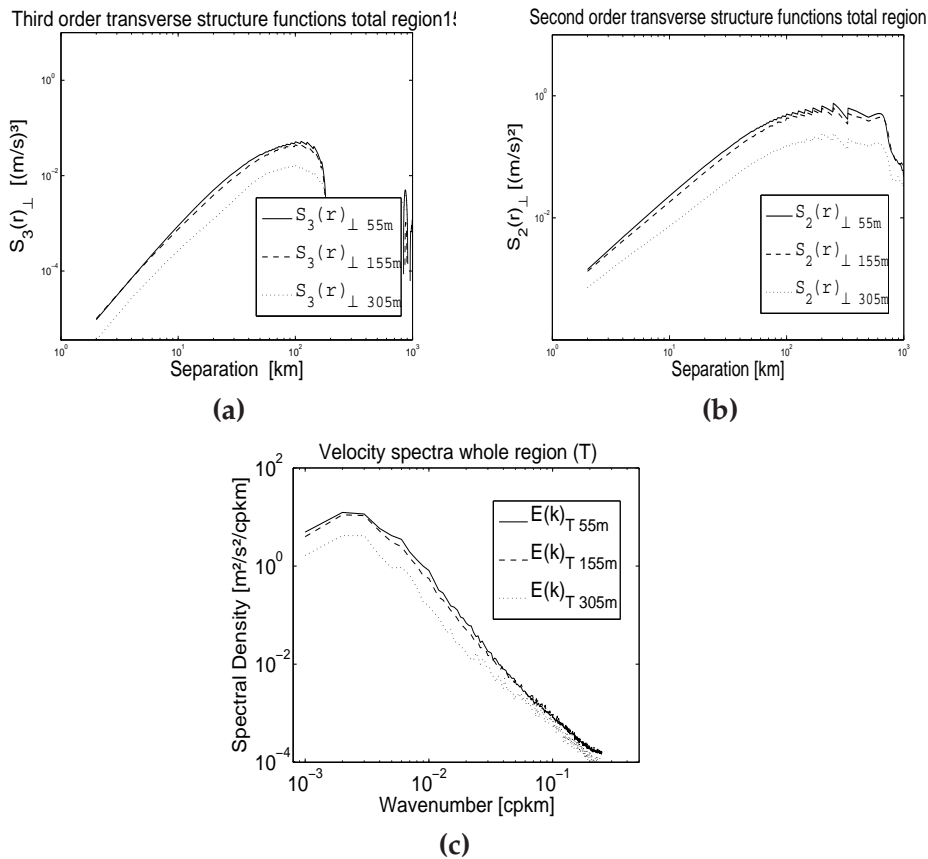
Figure 5.2: *Transverse components of velocity spectra (a), second (b) and third order (c)*
structure functions obtained from 55 m (solid), 155 m (dashed) and 305 m
(dotted) Oleander data records.

velocity and second and third order structure function at different depths
5.2, show that the results are comparable within each region at all depths,

suggesting same turbulent dynamics are present down to 305m depth. However, the eastern region presents energy spectra and second order structure functions with less steep slopes. For the second order structure function this is considered as if it has started to roll earlier off the r^2 dependencies, but it is still there. The velocity spectra are considered noisy, but still it is arguably a slope near to -3. This will be further discussed in the next section.

5.2 Absence of $k^{-5/3}$ velocity spectra

From the two dimensional turbulence theory, a system which is forced at a short range of scales is expected to invoke two inertial ranges; one energy inertial range at scales larger than forcing scales, and one enstrophy inertial range at scales smaller than the forcing scales. In the energy range, the results obtained from the idealized model data presented velocity spectra of a $k^{-5/3}$, consistent with the energy flux measures indicating an upscale energy cascade. However, the second order structure functions did not show a clear range with the corresponding $r^{2/3}$ dependence. Thereby, it could be that even though the results obtained from Oleander data did not show a clear range with $r^{2/3}$ dependence for the second order structure functions, there could be an upscale energy cascade. However, the velocity spectra obtained from the Oleander data did not exhibit a $k^{-5/3}$. How should these results be interpreted? And where are the forcing scales in the ocean in order to determine what scales are larger or smaller than the forced scales? First, the flatter the second order structure functions at larger scales are discussed, therafter, a discussion around the expected forcing scales in the ocean.

Second order structure functions rolling behavior

In figure 5.3 the second order structure functions are illustrated with a horizontal line indicating the variance of the longitudinal velocity. It can be seen that the curve asymptotes towards this variance value. This can be explained by taking a closer look at the second order structure function.

$$< (u(x+r) - u(x))^2 > = < u(x+r)^2 > + < u(x)^2 > - 2 < u(x+r)u(x) > \quad (5.1)$$

For large separations, the last term of equation (5.1) is zero. This is because the two velocities will be far apart and have no correlation. Thus, what is left in (5.1) is two times the variance of u. From this observation it can be argued that the curves are rolling off the enstrophy relation of r^2 towards the asymptote of the variance, and not towards a $r^{2/3}$ dependence. So the observations of the curves becom-

Second order structure functions eastern region

Figure 5.3: $S_2(r)$ at with variance of the longitudinal component (dashed black line).

ing flatter, does not necessarily mean that there is a sign of an upscale energy cascade.

Forcing scales

In the ocean, the mesoscale eddies (10-100 km) are believed to be forced primarily by baroclinic instability (Robert B. Scott, 2005)(Holton, 2004), inherent in this region of measurements which allows extraction of energy from the environmental potential energy reservoir. From the Eady model (Eady, 1949) it is deducted that there is a whole range of waves growing. But the fastest growing wave (the one which gets the most energy from the reservoir), scales as deformation radius which is approximately 30 km (120 km wavelengths) in the latitudes of the region of measurements (figure 5.2). Considering these arguments, it could be argued that the ocean is expected to present an energy range with its corresponding $k^{-5/3}$ velocity spectrum at scales above the deformation radius.
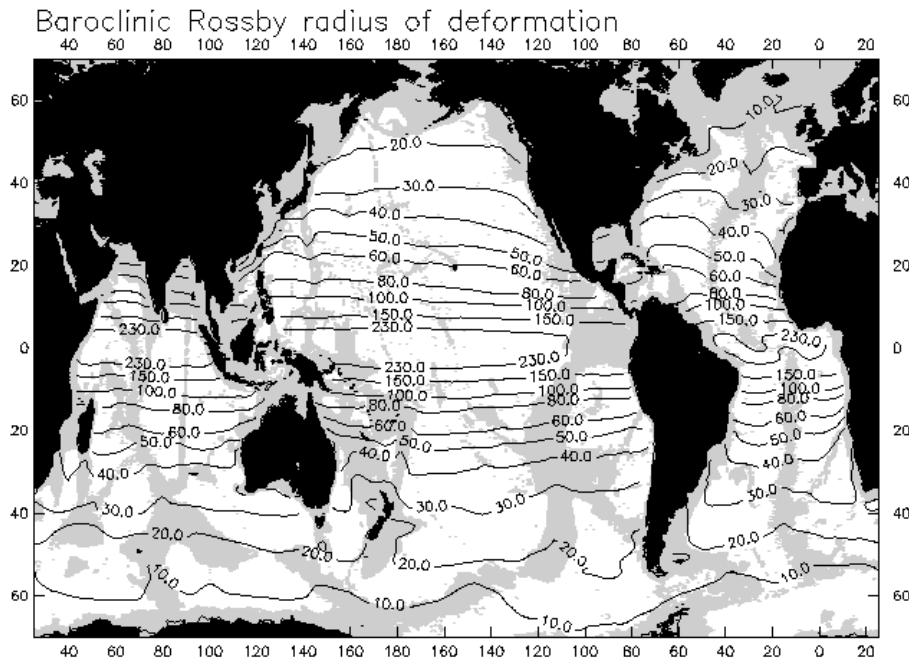

Figure 5.4: Deformation radius of the ocean. $From http : //www - po.coas.oregonstate.edu/research/po/research/rossby_radius/index.html$.

Velocity spectra

The velocity spectra obtained from the Oleander data exhibit no clear range of $k^{-5/3}$ dependence at the scales above the deformation radius. However, the peak of the energy spectra are at scales larger than the deformation radius. Thereby, based on forcing at scales of deformations radius, this could suggest that there is an upscale energy cascade from these forced scales up to the scales invoking the peak in the velocity spectra (200 km wavelengths) (Larichev and Held, 1995). If these suggestions are correct, we don't have any explanation for the absence of the $k^{-5/3}$. It could also be suggested that the peak sin the velocity spectra are caused from direct forcing at those

scales (e.g. by the Gulf Stream pinching off rings).

Considering the smallest scales, it could be argued that the spectral slopes are between -5/3 and -3. In order for an upscale energy cascade to be present at these scales, a source of energy is needed at even smaller scales, maybe in the order of a few km wavelengths. We could not find any evidence of, nor suggestions of, forcing mechanism at such small scales.

5.3   Fluxes

The Oleander dataset is one dimensional. Thus, we could not measure the fluxes directly (chapter 3). However, we can make inferences about them indirectly by considering the third order structure functions. The third order structure functions exhibit r^3 dependencies and are positive at scales below 40 km. From equation (2.83), these results suggest there is a downscale enstrophy flux.

In addition, considering the results from the model data calculations, r^3 third order structure function and a r^2 second order corresponded to a downscale enstrophy flux.

Chapter 6

Summary and conclusion

The main purpose of this thesis has been to investigate the turbulent dynamics in the upper ocean. We used statistical methods with direct oceanic measurements in the upper Atlantic ocean. The results obtained by applying the methods were compared to the results predicted by two dimensional turbulence theory.

Prior to analyzing the ADCP data from the oceanic measurements, they were subject to a screening process in order to secure high data quality. Further, the research was conducted in three regions in the horizontal; the eastern, western and the total region of measurements. In addition, these three regions were analyzed at three depths; 55 m, 155 m and 305 m.

Structure functions and velocity spectra were applied in the analysis. These methods were tested on a data set obtained from a two dimensional model run, providing results which showed good agreement with the predicted results from two dimensional turbulence theory.

The results obtained from the Oleander data set reveal that the assumption of homogeneity is arguably held and the assumption of isotropy is reasonably held in all the three regions, at all three depths, for scales below the deformation radius (30-40 km).

For isotropy, this is based on the fact that the second order isotropic relation was held in all regions at all depths below scales of the deformation radius. For homogeneity, this is based on the fact that the second order structure functions were arguably similar in all regions at each depth. In addition, the velocity spectra were arguably similar at each depth. Noticeably, third order structure functions presented some results which could break both assumptions. These contradicting results from the eastern region could be explained by the intermittency effects, causing slow statistical convergence for the third order structure functions. Nevertheless, the results of

the second order structure functions and velocity spectra are not distrusted.

The results obtained from the Oleander data set are all in all in reasonable accordance with the structure functions and velocity spectra corresponding to an enstrophy cascade below the scales of deformation radius. Above scales of the deformation radius, a clear sign of an upscale energy cascade was not revealed by the methods applied on the Oleander dataset.

Below the deformation radius, the results can be interpreted as to imply that the there is enstrophy cascade. Therefore the results from this study can be interpreted as to give support to the two dimensional turbulence theory rather than surface quasi-geostrophy.

Future work

From the results of this thesis, it is clear that further theoretical and field research is needed in order to create consensus among scientists regarding the turbulence dynamics of the upper ocean. Some ideas for future work are listed below.

- Undertake a project where direct oceanic data and satellite altimetry data are simultaniously measured over the same area at the same time. This will make it possible to evaluate if there is noise in the altimetry data, as suggested by (Wang et al., 2010).

- In order to estimate the fluxes with direct oceanic measuremtents, a two dimenional data set is required. It would be of great value to estimate such measures. This could maybe be done by applying a horizontal ADCP to profile the oceanic currents in the horizontal simultaniously as in the vertical.

Bibliography

() .

Batchelor, G.K. (1953) *T*he theory on homogeneous turbulence (Cambridge University Press).

Batchelor, G.K. (1969) *Computation of the energy spectrum in homogeneous two-dimensional turbulence*. Physics of Fluids, Vol. 12B: p. 233–239.

Bennet, A. F. (1984) *Relative dispersion: Local and non-local dynamics. J. Atmos. Sci. 41,.* J. Atmos Sci, Vol. 42: p. 1881–1886.

Boffetta, G. (2007) *E*nergy and enstrophy fluxes in the double cascade of two-dimensional turbulence. JOURNAL OF FLUID MECHANICS, Vol. 589: p. 253–260.

Charney, Jule G. (1971) *G*eostrophic Turbulence. Journal of the Atmospheric Sciences, Vol. 28(6): p. 1087–1095.

Eady, E. (1949) *LONG WAVES AND CYCLONE WAVES*. TELLUS, Vol. 1(3): p. 33–52.

Flagg, CN; Schwartze, G; Gottlieb, E and Rossby, T (1998) *O*perating an acoustic Doppler current profiler aboard a container vessel. JOURNAL OF ATMOSPHERIC AND OCEANIC TECHNOLOGY, Vol. 15.

Frisch, Uriel (1995) *T*urbulence the legacy of A.N Kolmogorov (Cambrigde University press, Cambrigde, England).

Gage, KS (1979a) *evidence for a k-5-3 law inertial range in mesoscale 2-dimensional turbulence*. JOURNAL OF THE ATMOSPHERIC SCIENCES, Vol. 36(10): p. 1950–1954.

Gage, K.S. (1979b) *Evidence for a k-5-3 law inertial range in mesoscale two-dimensional turbulence*. Journal of Atmospheric Sciences, Vol. 36: p. 1950–1954.

Gage, K.S. and Nastrom, G.D. (1986) *T*heoretical interpretation of atmospheric wavenumber spectra wind and temperature observed by commercial aircraft during GASP. Journal of Atmospheric Sciences, Vol. 43: p. 729–740.

Holton, James R. (2004) *A*n introduction to dynamic metereology (Department of Atmospheric Science, University of Washington).

Kolmogorov, A.N. (1941) *The local-structure of turbulence in incompressible viscous-fluid for very large reynolds-numbers*. Doklady Akademii Nauk SSSR, Vol. 30: p. 9–13.

Kraichnan, R.H. (1967) *Inertial ranges in two dimensional turbulence*. Physics of Fluids, Vol. 10: p. 1417–1423.

Kraichnan, R.H. (1970) *Inertial-range transfer in two- and three-dimensional turbulence*. J. Fluid Mech., Vol. 47: p. 525–535.

LaCasce, J. H. (2008) *Statistics from Lagrangian observations*. PROGRESS IN OCEANOGRAPHY, Vol. 77(1): p. 1–29.

LaCasce, JH (2002) *On turbulence and normal modes in a basin*. JOURNAL OF MARINE RESEARCH, Vol. 60(3): p. 431–460.

Lacasce, J.H. (2010) *I*nstability and turbulence,lecture notes (Department of Geosciences, University of Oslo).

LaCasce, J.H. (2010) *Pair separations in the 2-D turbulent enstrophy range*. Phys. Fluids, (in prep).

Larichev, VD and Held, IM (1995) *eddy amplitudes and fluxes in a homogeneous model of fully-developed baroclinic instability*. JOURNAL OF PHYSICAL OCEANOGRAPHY, Vol. 25(10): p. 2285–2297.

Le Traon, P. Hua Bach Lien Dibarboure G., P. Y. Klein () *Do altimeter wavenumber spectra agree with the interior or surface quasigeostrophic theory*.

Lindborg, E (1995) *Kinematics of homogeneous axisymmetrical turbulence*. JOURNAL OF FLUID MECHANICS, Vol. 302: p. 179–201.

Lindborg, E (1999) *Can the atmospheric kinetic energy spectrum be explained by two-dimensional turbulence?*. JOURNAL OF FLUID MECHANICS, Vol. 388.

Nastrom, G.D. and Gage, K.S. (1984) *A* climatology of atmospheric wavenumber spectra of wind and temperature observed by commercial aircraft. Journal of Atmospheric Sciences, Vol. 42: p. 950–960.

Pope, Stephen B. (2000) *T*urbulent flows (Cambridge University Press).

Richardson, Lewis Fry (1922) *W*eather Prediction by Numerical Process (Cambrigde University press, Cambrigde, England).

Rivera, MK; Daniel, WB; Chen, SY and Ecke, RE (2003) *Energy and enstrophy transfer in decaying two-dimensional turbulence*. PHYSICAL REVIEW LETTERS, Vol. 90(10).

Robert B. Scott, Faming Wang (2005) *Direct evidence of an Oceanic Inverse Kinetic Energy Cascade from satellite Altimetry*. JOURNAL OF PHYSICAL OCEANOGRAPHY, Vol. 35.

Salmon, R (1980) *Baroclinic instability and geostrophic turbulence*. GEOPHYSICAL AND ASTROPHYSICAL FLUID DYNAMICS, Vol. 15(3-4): p. 167–211.

Schneider, T and Walker, CC (2006) *Self-organization of atmospheric macroturbulence into critical states of weak nonlinear eddy-eddy interactions*. JOURNAL OF PHYSICAL OCEANOGRAPHY, Vol. 63(6): p. 1569–1586.

Stammer, D (1997) *Global characteristics of ocean variability estimated from regional TOPEX/POSEIDON altimeter measurements*. JOURNAL OF PHYSICAL OCEANOGRAPHY, Vol. 27(8): p. 1743–1769.

Vallgren, Andreas and Lindborg, Erik (2010) *Charney isotropy and equipartition in quasi-geostrophic turbulence*. JOURNAL OF FLUID MECHANICS, Vol. 656: p. 448–457.

Vallis, G.K. (2005) *A*tmospheric and oceanic fluid dynamics (Available from www.princeton.edu/ gkv/aofd. (To be published by Cambridge University).

Van Atta, Chen W. Y., C. W. (1970) *Structure functions of turbulence in the atmospheric boundary layer over the ocean.* JOURNAL OF FLUID MECHANICS, Vol. 44: p. 145–159.

Wang, Dong-Ping; Flagg, Charles N.; Donohue, Kathleen and Rossby, H. Thomas (2010) *Wavenumber Spectrum in the Gulf Stream from Shipboard ADCP Observations and Comparison with Altimetry Measurements.* JOURNAL OF PHYSICAL OCEANOGRAPHY, Vol. 40(4): p. 840–844.